IEEE Access
Multidisciplinary ⋮ Rapid Review ⋮ Open Access Journal

Received 29 June 2023, accepted 14 July 2023, date of publication 20 July 2023, date of current version 26 July 2023.

Digital Object Identifier 10.1109/ACCESS.2023.3297136

RESEARCH ARTICLE

Rule Design for Interpretable En Route Arrival Management via Runway-Flow and Inter-Aircraft Control

KATSUHIRO SEKINE[1], FURUTO KATO[2], TOMOAKI TATSUKAWA[1], (Member, IEEE), KOZO FUJII[1], (Member, IEEE), AND ERI ITOH[2,3,4]

[1]Department of Information and Computer Technology, Tokyo University of Science, Tokyo 162-8601, Japan
[2]Department of Aeronautics and Astronautics, The University of Tokyo, Tokyo 113-8656, Japan
[3]Air Traffic Management Department, Electronic Navigation Research Institute, Tokyo 182-0012, Japan
[4]Research Center for Advanced Science and Technology, The University of Tokyo, Tokyo 153-8904, Japan

Corresponding author: Eri Itoh (eriitoh@g.ecc.u-tokyo.ac.jp)

This work was supported in part by JSPS KAKENHI under Grant 20H04237 and Grant 22J22970; and in part by the Collaborative Actions for Renovation of Air Traffic Systems (CARATS) through the Japan Civil Aviation Bureau (JCAB) of the Japanese Ministry of Land, Infrastructure, Transport, and Tourism.

ABSTRACT There are ongoing research efforts to implement En route arrival manager (AMAN), which decides arrival runways and controls cruise speed in en route airspace. Air traffic control operations that regulate arrival air traffic flows from en route airspace are considered effective in mitigating the congestion close to destination airports. Therefore, this study proposes a scientific system design for operationally feasible En Route AMAN assisting air traffic controllers (ATCos) through runway-flow and inter-aircraft control. Herein, we devise an airline-oriented runway assignment rule that selects a target minimizing arrival taxi time in case of over-demand according to the maximum estimated through the stochastic distribution of inter-aircraft time and runway occupancy time. We also formulate speed control rules based on inter-aircraft spacing using simulation-based optimization and decision tree analysis to visualize the distinct strategies and rules for the traffic responsible for each ATCo. Furthermore, an agent-based simulation is performed to evaluate the system effectiveness in reducing the arrival delay. The simulation indicates 20-d arrival and departure at the Tokyo International Airport, Japan, between 06:00 and 23:00. The results show that the designed IF–THEN rules reduce the total arrival sequencing delay time and arrival taxi time by 21% (median, 55.8 s) and 6.9% (median, 24.6 s). Our findings suggest that truly optimal scheduled time of arrival (STA) and operationally feasible rules for ATCos could promise congestion relief while ensuring the interpretability and possibility of En Route AMAN implementation.

INDEX TERMS Agent-based simulation, air traffic control, arrival management, data-driven approach, decision tree analysis.

I. INTRODUCTION

Arrival MANager (AMAN) is a general term for safely and effectively arranging arrivals smoothly for landing at a destination airport [1]. As a family of decision support systems, AMANs assist air traffic controllers (ATCos) to improve the arrival management process. According to [1], AMAN is a specifically designed software used to help metering and sequencing arrival streams and provide the information needed for efficient arrival management. To accommodate the increasing air traffic demand [2], so-called En Route AMAN, which perform runway assignment and speed control in en route airspace, is being designed to loosely coordinate with the current AMAN.

In the United States, a Traffic Management Advisor (TMA) [3] was deployed in air traffic control (ATC) centers in the 1990s. Since then, TMA has been improved under the NextGen program [4]: Time-Based Flow Management (TBFM) [5] in en-route airspace and Terminal Sequencing and Spacing (TSAS) [6] in terminal airspace.

The associate editor coordinating the review of this manuscript and approving it for publication was Fabrizio Messina.

These systems contributed toward consistently sequencing and time-spacing the arrival traffic in en route and terminal airspace areas. Currently, autonomous airborne separation control among aircraft, known as flight-deck interval management (FIM) [7], is being implemented. In Europe, the Single European Sky ATM Research (SESAR) project [8] has facilitated the collaboration among European countries and contributed to the development of cross-border arrival management, which coordinates arrival time schedules covering more comprehensive ranges of airspace than those in conventional operations [9]. In Asia-Pacific, a report targeting the strategic air traffic flow management (ATFM) region devised long-range ATFM (LR-ATFM) to provide a basis for research into the application beyond the current system time frames [10]. In Japan, the research program of the En Route AMAN has been conducted by a study group in collaboration with the Japan Civil Aviation Bureau (JCAB) under Collaborative Actions for Renovation of Air Traffic Systems (CARATS) [11], with the goal of maintaining an efficient traffic flow at the Tokyo International Airport [12]. Regional research and development increased the need for a scientific method to design and implement En Route AMANs according to the characteristics of the target airports, airspace, and air traffic flow.

Traditionally, for aircraft arrival management, the focus in academia has frequently been on extending the runway scheduling problem, wherein the runway assignment, sequencing, and spacing are mathematically formulated and are solved quickly using optimization method. In the optimization problem, various objective functions are considered depending on the decision makers (airport and airline operators, and governments), with most studies generally aiming to increase runway capacity from the airport's perspective and maximizing on-time performance and minimizing fuel consumption from the airline's perspective. The exact solution approach including mixed-integer programming [13], [14] and dynamic programming [15], [16] can obtain optimal solutions within a short computation time while flexibly incorporating various operational constraints and separation requirements on multiple runways. Conversely, the stochastic optimization methods, such as genetic algorithm [17], [18], simulated annealing [19], [20], tabu search [21], [22], and ant colony optimization [23], [24], can update solutions according to the dynamic changes in the schedule within a short computation time. Compared with the model-free and learning-based scheduling methods such as reinforcement learning [25], [26], arrival sequencing and spacing rules are relatively clear, attracting considerable interest. However, these existing runway scheduling algorithms assume that the scheduling inputs are known and hence, did not consider various uncertainties such as weather, human factors, delay propagation, and radar appearance errors. Moreover, the air traffic flow environment considered in the traditional studies only focuses on maximizing the runway throughput, thereby possibly overlooking the bottlenecks excluding the runways when extending the planning horizon.

Recent research has proposed sophisticated algorithms, which are resistant to uncertainty while incorporating the characteristics of air traffic flow. Jones et al. [27] proposed an optimization method using stochastic programming to adjust the arrival times of waypoints representing each node in a network traffic flow model. Their proposed model achieved a delay transfer from downstream to upstream airspace by 12.58% to 19.53%, targeting 500 NM centered at the Hartsfield–Jackson Atlanta International Airport, the United States. Meanwhile, Khassiba et al. [28] proposed a runway scheduling model called the two-stage stochastic algorithm, which aimed to exclusively optimize the arrival time at the initial approach fix (IAF) corresponding to the stage boundary. The authors extended this idea using chance-constrained stochastic programming to limit the risk of IAF separation violation [29] and considering the multiple IAFs with different time deviation according to aircraft type and flight phase [30]. In [28], a time-based simulation model for the Paris Charles de Gaulle International Airport, France, showed that the proposed method reduced conflicts in the terminal area by 73.5% compared with the baseline scenario. This multistage arrival management was found in [31], where Schultz et al. developed an LR-ATFM operational concept using the k-means clustering method, kernel density estimation, and linear programming. They proposed a speed control concept targeting the arrival time at IAF (Target Time Over in [31]) of Changi International Airport, Singapore, demonstrating a reduction in the total holding aircraft number and holding time by 26.5% and 28.3%, respectively. Jun et al. [32] proposed the Extended AMAN, which detected the holding stack via machine learning and dynamically applied speed control at 500, 400, and 300 NM using the heuristic optimization, achieving 65% delay reduction at the same target airport.

The abovementioned studies have contributed to effective delay transfer from the terminal airspace to the en route airspace while capturing the traffic characteristics, realizing a smooth whole arrival traffic flow. However, most existing studies compute the scheduled time of arrival (STA), compelling air traffic controllers (ATCos) to provide guidance instructions that minimize the difference against the estimated time of arrival (ETA). Because of the large ETA error, this type of operation changes the arrival order and the amount of time adjustment during congestion, increasing the operational procedures of ATCos, and is often operationally infeasible. Conversely, studies in [33], [34], [35], and [36] proposed the inter-arrival time control as an alternative to STA control and evaluated the effectiveness on the basis of the queuing theory. In [33], a $G/G/c$ queuing model analysis of airport arrival delays was performed using two years of radar tracks and flight plans at the Tokyo International Airport (RJTT). Results showed that the transition from flow control to arrival time management enhanced the airspace capacity. Because the required inter-arrival times (separation minima) between the aircraft and airspace capacity are constraints, the extended model [34] revealed bottlenecks

wherein controlling inter-arrival times can reduce delay times. The $M/G/c/K$ queuing model [35] was used to evaluate the different tactical control strategies for RJTT arrivals at 100 NM around the airport by considering the service time and its variance within the suggested airspace. Consequently, the arrival strategies improved with a new wake turbulence separation minima. Integrating nonlinear integer programming and the $G_t/GI/s_t + GI$ fluid queuing model with the time-varying arrival rate, [36] demonstrated that controlling the inter-aircraft time reduced the arrival traffic delay at RJTT by 18.8% on average. To apply this concept practically, the En Route AMAN strategies and rules that are operational in the actual field of ATC should be scientifically designed.

As the next step toward the implementation of En Route AMAN, the objective of this study is to comprehensively design strategies and rules for runway assignment and speed control interpretable for ATCos responsible for each airspace. Accordingly, this paper proposes a concept and a design method for an AMAN (called flow-based En Route AMAN) that controls the inter-arrival time of the en route airspace with a constraint on the maximum number of arrivals at the runway per hour. The runway flow is defined as the number of aircraft using a runway in a time window, and runway reassignment occurs when the maximum number is exceeded. Although this concept of flow is conventionally used in ATFM [31], this study applies it to En Route AMAN to deal with the uncertainty of ETA. Runway reassignment makes the proposed approach applicable to large-scale airports with multiple runways. The airline-oriented runway assignment rule selects the target that minimizes the taxiing time at an airport. We use simulation-based optimization and data exploration techniques to devise the speed control rules. Our aim is to discover strategies and extract knowledge and rules based on inter-aircraft control originating from the existing studies applying the queuing theory [33], [34], [35], [36].

This paper is organized as follows. Section II proposes the concept and principle of a flow-based En Route AMAN using runway-flow and inter-aircraft control. Section III gives a brief overview of the stochastic characteristics of airspace and surface traffic at RJTT as one of the case studies of Section II. To crystallize the concept and principle proposed in Section II, Sections IV and V analyze the optimal runway assignments and speed control rules for the case study of airport demonstrated in Section III. To validate the rules devised in Sections IV and V, we perform a four-dimensional (4D)-trajectory- and agent-based simulation in Section VI. Finally, Section VII discusses the results obtained in Sections IV, V, and VI and compares them with previous studies mentioned in Section I.

II. DESIGNING FLOW-BASED EN ROUTE AMAN

A. DESIGN CONCEPTS

The concept of designing flow-based En Route AMAN proposed herein is shown in Fig. 1. As mentioned in Section I, this En Route AMAN targets large-scale airports with multiple runways shared by takeoff and landing aircraft. The main function comprises two parts: (1) runway assignment and (2) speed control. The data inputted into the runway assignment function are as follows.

- Possible takeoff time (PTOT) estimated by Departure MANager (DMAN).
- ETA lists predicted using flight time from en route airspace to runway threshold.
- Statistic data of the maximum arrival/departure rate on a runway.
- Information/data required to decide rules for arrival sequencing and delay assignment.

First, the runway assignment function predicts the "short-term" runway flow by calculating the arrival/departure slots based on PTOT and ETA. When the calculated value exceeds the maximum number of slots, an arrival flight is reassigned to another runway. Then, the runway assignment function decides the arrival runway of the arrival flight lists, including the call sign, ETA, and arrival runway, which are the outputs of this function. After controlling the influx traffic within a time frame by the runway assignment function, the speed control function decreases the variance in the arrival sequence by controlling the inter-aircraft spacing in the time axis. To achieve the best inter-aircraft coordination, we need information/data to decide the optimal rules for speed control in en route airspace in addition to the output of the runway assignment function. Therefore, under the hypothesis that airspace other than runways will also be a bottleneck, the airspace bottlenecks are analyzed before applying the speed control rule. According to this rule, sequencing delay originating from the terminal airspace is transferred to the en route airspace, which minimizes terminal congestion. Finally, the speed control target can be obtained with the command advisory instructed in the en route airspace. The detailed principle of each function is explained in the following subsections.

B. RUNWAY ASSIGNMENT PRINCIPLE: INFLOW CONTROL

As shown in Fig. 1 (see the middle-top component), our proposed approach uses the parameters and variables listed in Table 1. The key parameters are time frame (ξ) and the

TABLE 1. List of symbols and descriptions: runway assignment principle.

Symbol	Description
$t_{ETA,RWY}$	Set: estimated time of arrival (ETA) at the runway threshold (RWY), which is predicted at a waypoint FIX_i.
$t_{PTOT,RWY}$	Set: possible takeoff time (PTOT) at the RWY predicted at a waypoint FIX_i.
ξ	Parameter: the time frame assigned to count arrival aircraft (slots at the runway).
$N_{max/\xi,RWY}$	Parameter: maximum arrival slots in ξ.
$t^{@}_{ETA,RWY}$	Variable: ETA of the target arrival aircraft at RWY, which just cross over FIX_i.
$N_{\xi,RWY}$	Variable: arrival aircraft numbers satisfying $[t^{@}_{ETA,RWY} - \xi, t^{@}_{ETA,RWY}] \in t_{ETA,RWY}$.
$t_{i,RWY}$	Variable: the time frame ξ for RWY.

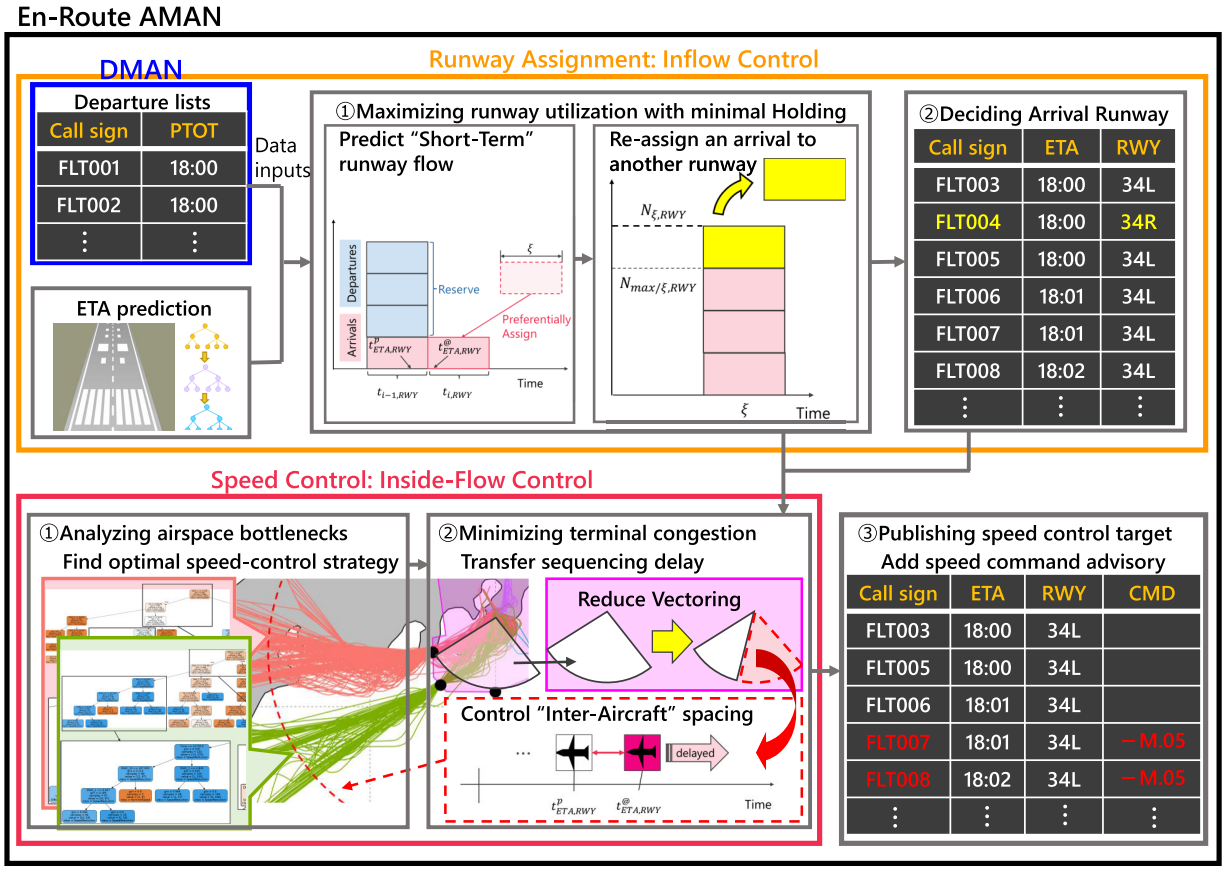

FIGURE 1. Conceptual diagram of a flow-based En Route AMAN equipped with two functions: (1) runway assignment function counts short-term departure/arrival slots and reassigns the excess arrivals to another runway; (2) speed control function reduces the variance in the arrival sequence to minimize the terminal congestion.

maximum arrival slots ($N_{max/\xi,RWY}$). Basically, slots in ξ are assigned by giving priority to arriving aircraft that have limited time to adjust in the air. However, $N_{max/\xi,RWY}$ is set to avoid an excessive queue of departure aircraft, and any excess is allocated to another runway. Several factors, such as wake turbulence categories, safety margins, and runway occupancy time (ROT), affect $N_{max/\xi,RWY}$, so it is estimated using a stochastic approach (see Sec. IV). After deciding $N_{max/\xi,RWY}$, the En Route AMAN system is opened the reservation to airlines; this reservation is required for departure in the time frame $t_{i,RWY}$. $t_{PTOT,RWY}$, estimated by the DMAN system, is used to assign the departures in $t_{i,RWY}$. Once the takeoff and landing rates are determined, speed control is applied to reduce the variance within the time frame, thereby reducing the delay in the terminal maneuvering area.

C. SPEED CONTROL PRINCIPLE: INSIDE-FLOW CONTROL

The speed control principle described in Fig. 1 (see the bottom-middle component) works with the parameter and variables listed in Table 2. The speed control is implemented to minimize the variance in inter-aircraft time calculated as follows.

$$t^{@}_{ETA,RWY} - t^{p}_{ETA,RWY}. \tag{1}$$

TABLE 2. List of symbols and descriptions: speed control principle.

Symbol	Description
$t_{ETA,RWY}$	Set: estimated time of arrival (ETA) at the runway threshold (RWY) predicted at a waypoint FIX_i.
τ	Parameter: inter-aircraft time between the target arrival aircraft and its preceding aircraft.
$t^{@}_{ETA,RWY}$	Variable: ETA of the target arrival aircraft at the RWY, which just cross over FIX_i.
$t^{p}_{ETA,RWY}$	Variable: ETA of the aircraft preceding the target arrival one.

Our En Route AMAN provides the speed control advisory when the parameter τ exceeds the relative time interval between the target aircraft and its preceding aircraft instead of using STA. Traditional research typically focuses on optimizing runway throughput only, ignoring other aspects of the airport airspace, which are unique to each airport and also contribute to congestion. Therefore, this study applies a more realistic approach considering the traffic volume and the specific structure of the route to obtain the optimal speed control rule according to the target airport and airspace (see Sec. V). For the implementation of our En Route AMAN, concretizing the concept and principle depending on airport and airspace is a paramount process. Therefore, this study proposes an approach to the strategy and rule design for

runway assignment and speed control principle focusing on RJTT as a case study airport.

III. AIRSPACE AND SURFACE TRAFFIC AT A CASE STUDY AIRPORT: TOKYO INTERNATIONAL AIRPORT (RJTT)

A. RUNWAY CONFIGURATION

In 2019 [37], RJTT was ranked as the fifth busiest airport in the world in terms of passenger traffic, which is about 85.50 million. The annual number of aircraft movements is approximately 458,368, and it is designated as "Level 3," the most congested level in the Worldwide Airport Slot Guideline of the International Air Transport Association [38].

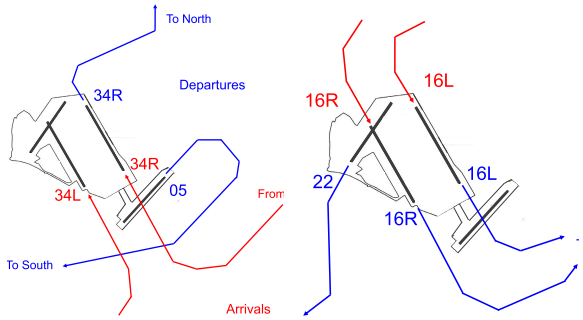

(a) Northerly wind operation (b) Southerly wind operation

FIGURE 2. Runway configuration at RJTT.

The airport uses four runways: a set of parallel from north to south runways (34L/16R and 34R/16L) and two southwest-to-northeast crosswind runways (22/04 and 23/05). Fig. 2 shows the runway configuration of departure and arrival traffic in RJTT, which depends on the direction of the wind. In northerly wind operation, aircraft arrive at runway 34L or runway 34R, whereas departure flights take off from runway 05 or runway 34R, according to their origin/destination airports, as shown in Fig. 2(a). Runway 34R is used as the departure–arrival mixed mode for northbound traffic, whereas runways 05 and 34L are used for only departure and arrival for southbound traffic, respectively. Meanwhile, as shown in Fig. 2(b), southerly wind operation uses runways 16L and 16R for northbound departures and arrivals in both northbound and southbound traffic, while using runway 22 for southbound departures. The statistic shows that northerly wind operation occupies a large percentage of the total, approximately 70% of all yearly departure and arrival traffic. Therefore, this paper focuses on the northerly wind operation, especially the runway used only for arrival, that is, runway 34L.

B. AIRSPACE OPERATION

This study analyzes arrival flights extracted from the flight plan (FP) and radar track (RD), which are selected for a period of 39 days from one week of each month with the nominal condition of northerly wind operation between September 2019 and February 2020. FP includes the call sign and the routing structure of waypoints with the corresponding passing time and cruise altitude. RD is the time series trajectory data containing the time recorded for ∼10 s, the call sign; the latitude, longitude, altitude, and type of the aircraft. On average, there are 623 arrivals per day: 502 domestic and 121 international.

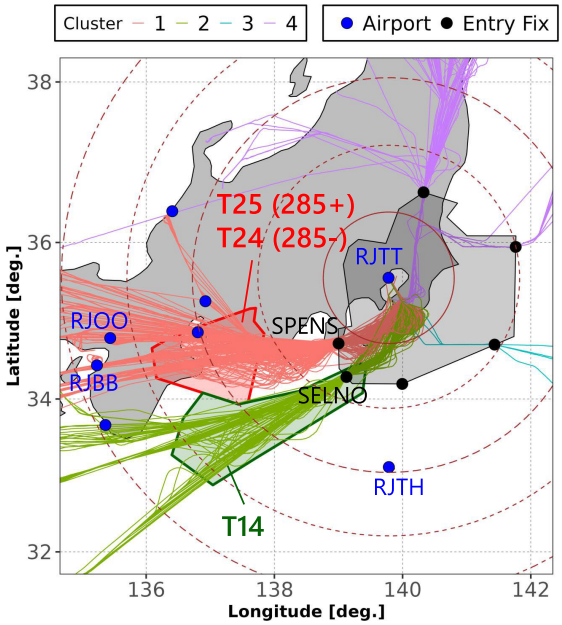

FIGURE 3. Actual radar tracks color-coded with four colors according to the direction bound for RJTT in the northerly wind operation on a day in December 2019. Tokyo approach control area is bounded by a black polygon with six entry fixes depicted with black dots. The radius of the brown dotted concentric circle is 50 NM centered on RJTT. The red polygon and green polygon show the en route sector in which the cruise speed control and the runway assignment decision are implemented. The blue dots indicate the airports located within 250 NM of RJTT. RJTT, Tokyo international airport; RJOO, Osaka international airport; RJBB, Kansai International Airport; and RJTH, Hachijojima Airport.

Fig. 3 shows the actual radar tracks of the arrival air traffic at RJTT under the northerly wind operation with the nominal traffic conditions. There are four clusters: clusters 1 through 3 include 472.7 flights per day coming from the southwest direction and basically landing on runway 34L, and cluster 4 (purple lines in the figure) has 151.2 flights per day coming from the north direction and basically landing on runway 34R. This means that the number of arrivals at runway 34L is more than three times that of arrivals at runway 34R. Cluster 3 (light blue lines) comprises three domestic flights per day from RJTH and five international flights from the Pacific Ocean (east of Fig. 3) and the Oceania region such as Australia (south of the figure). Compared to cluster 3, clusters 1 and 2 contain most southbound arrivals, 306.1 and 158.3 flights, respectively. Therefore, our study has focused on this traffic, considering cruise speed control and runway reassignment in T25 and T24 (red polygon in Fig. 3) and T14 (green polygon), 150 NM to 200 NM from RJTT. Furthermore, clusters 1 and 2 have 59.7 pop-up flights, which take off at the airport located within 250 NM of RJTT, negatively impacting the other traffic. In particular,

the pop-up flights departing from RJOO (29.9 flights/day) and RJBB (13.2 flights/day) cause spacing adjustments when they merge into the other traffic in cluster 1 (orange lines in Fig. 3). Another specific feature of clusters 1 and 2 is the path stretching just before entering the RJTT terminal airspace, called Tokyo Approach Control Area (TACA), to alleviate its over-demand. The entry fixes of clusters 1 and 2 are named SPENS and SELNO (black dots in Fig. 3), respectively.

After entering TACA, approach controllers implement the sequencing and spacing of the arrival traffic at runways 34L and 34R through the point-merge (PM) system [39]. As shown in Fig. 4, the configuration of PM routes is divided into ML-PM1 and ML-PM2 under the northerly wind operation. ML-PM1 and ML-PM2 comprise three and two overlapping PM routes located in the southern and northern areas, respectively, in addition to TACA. An arrival aircraft that enters the airspace flies over the sequencing leg on which a passing altitude is uniquely defined. Arrival aircraft flying on the sequencing leg are instructed to fly directly to the merge point when the distance to the preceding aircraft is ensured. As mentioned in Section III-A, inbound traffic coming from the southern and northern directions land on runways 34L and 34R, respectively. Therefore, ML-PM1 and ML-PM2 are basically segregated and independent. Meanwhile, the southbound arrival aircraft landing on runway 34R will pass through the outer area of ML-PM1 and enter ML-PM2 as shown in Fig. 4. Moreover, the northbound arrival aircraft merge beyond the merge point of ML-PM1 and land on runway 34L.

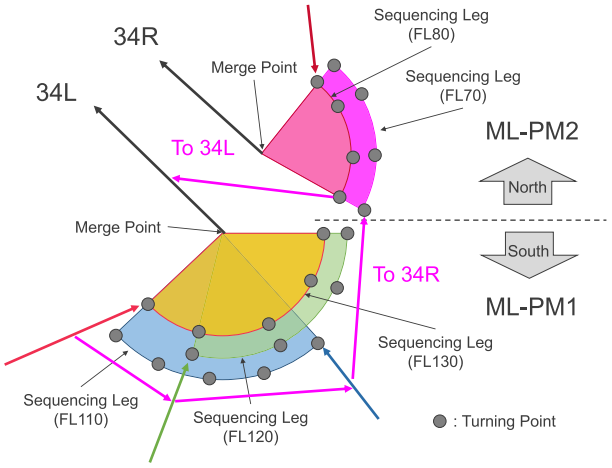

FIGURE 4. Schematic of the configuration of the point-merge (PM) system connected to 34L (multilevel point merge 1: ML-PM1) and 34R (multilevel point merge 2: ML-PM2) in tokyo approach control area (TACA) in the northerly wind operation.

C. SURFACE OPERATION

In addition to FP and RD, this study uses information from the spot assignment chart to determine the spot numbers and reference times of the aircraft departing RJTT. The JCAB of the Japanese Ministry of Land, Infrastructure, Transport, and Tourism donated all the data for the restricted use of this study.

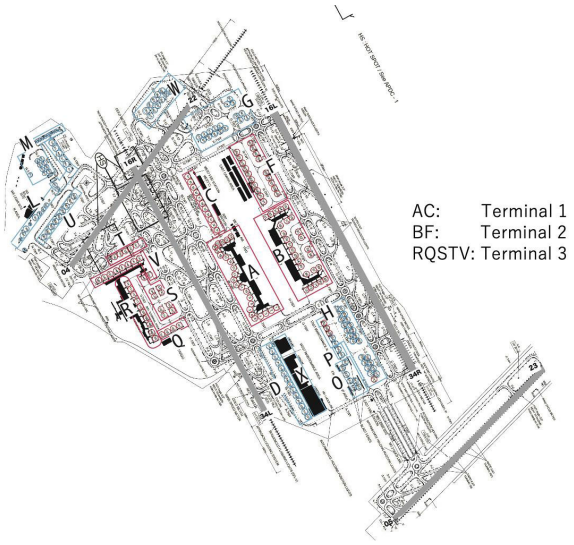

FIGURE 5. Surface configuration with terminal buildings, gates, and spots at Tokyo International Airport (RJTT).

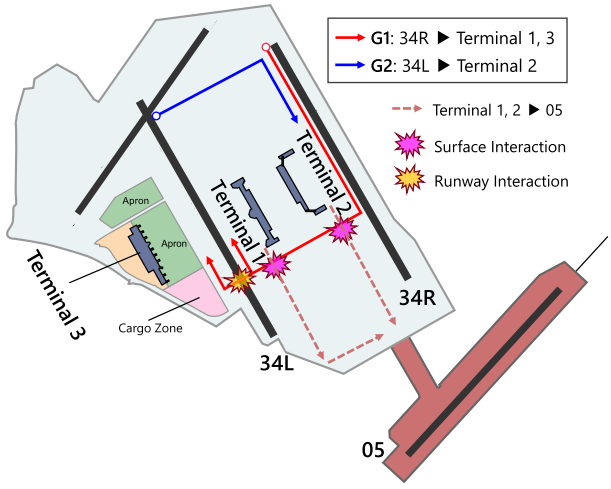

FIGURE 6. Long taxiing route for arrivals in northerly wind operation at Tokyo International Airport (RJTT). The long taxiing routes from runway 34R to terminals 1 and 3 (red lines; target group 1, G1) interact with the taxiing routes from terminals 1 and 2 to runway 05 (brown dotted lines). The blue line is a long taxiing route from runway 34L to T2 (target group 2, G2).

Fig. 5 shows the surface configuration, including terminal buildings and gate/spot groups. As shown in the figure, three terminals are located and numbered, to the east, as terminal 3 (T3), T1, and T2. The gates/spots are grouped and numbered from A to V: T1 contains A and C, T2 contains B and F, and T3 contains R, Q, S, T, and V. Domestic flights use T1 (41.2% of departures) and T2 (35.5% of departures), whereas international flights use T3 from R and V gates (11.4% of departures).

Fig. 6 shows the long taxi route on which the runway assignment-change targets run, together with the runway configuration of northerly wind operation at RJTT. Target

TABLE 3. List of symbols and descriptions: algorithm 1.

Symbol	Description
t_{ETA,ac_i}	Set: estimated time of arrival (ETA) of arrival sequence (AC) $(ac_1, ac_2, \cdots, ac_n, \forall i \in \{1, n\})$ at RWY34L and RWY34R at decision time t.
ξ	Parameter: the time frame assigned to count arrival aircraft (slots at the runway).
$N_{max/\xi,34L}$	Parameter: maximum arrival slots in ξ.
$N_{chg/h}$	Parameter: maximum number of the runway reassignments per hour.
$N_{h,34LtoR}$	Variable: number of aircraft assigned from RWY34L to RWY34R during hour h $(\forall h \in \{1, 24\})$ including time t_{ETA,ac_n}.
$N_{h,34RtoL}$	Variable: number of aircraft assigned from RWY34R to RWY34L during hour h $(\forall h \in \{1, 24\})$ including time t_{ETA,ac_n}.
$t^{@}_{ETA,34L}$	Variable: ETA of the target arrival aircraft at RWY34L, which just cross over FIX_i.
$N_{\xi,34L}$	Variable: arrival aircraft numbers satisfying $[t^{@}_{ETA,34L} - \xi, t^{@}_{ETA,34L}] \in t_{ETA,ac_i}$.

group 1 (red line, G1) is assumed to be arrival flights that land on runway 34R and cross the runway to reach T3 or T1. This G1 interferes with departures from T1 and T2 to runway 05 in the south of T1 and T2, causing the surface delay time. Moreover, the T3 arrivals of G1 cross runway 34L before reaching spots/gates, deteriorating the runway throughput for arrivals. Therefore, G1 should be assigned to runway 34L in terms of uncertainty reduction. However, runway 34L is already in high demand as it is used for southbound traffic, which dominates ∼70% of the total arrivals; therefore, considering runway assignment only from 34R to 34L is unacceptable. In terms of punctuality, target group 2 (blue line, G2) should be the best solution to avoid over-demand of runway 34L. In the northerly wind operation, the flights that are assumed to be landing on 34L will come from the southwest direction and will finally arrive at T2, experiencing long taxiing duration.

IV. DEVISING RUNWAY ASSIGNMENT RULE

The runway assignment rules are optimally designed by combining stochastic estimation and data-driven analysis. The design target is focused on runway 34L because 70% of the arrivals are coming from the south and are landing on this runway.

Algorithm 1 shows the runway assignment rule optimally designed for runway 34L using the attributes listed in Table 3. As conceptualized in Sec. II, ξ and $N_{max/\xi,34L}$ are the key parameters of the inflow control rule on runway 34L. When $N_{\xi,34L}$ exceeds $N_{max/\xi,34L}$, the target arrival of G2 is reassigned from runway 34L to runway 34R as shown in line 5 of Algorithm 1. Meanwhile, the target arrival of G1, which experiences the longest taxiing time, is reassigned from runway 34R to runway 34L if $N_{\xi,34L} \leq N_{max/\xi,34L}$ functions in line 11 of Algorithm 1. This reassigning algorithm based on the flow in runway 34L maximizes the runway throughput, making use of the full potential. However, frequent runway reassignments can reduce delays in the terminal area while increasing the task volumes of approach controllers. Moreover, the runway reassignment based on runway 34L, which

Algorithm 1 En Route AMAN Runway Assignment Rule

Input:
t_{ETA,ac_i} $(\forall i \in \{1, n\})$, ▷ decision target is ac_n.
ξ, $N_{max/\xi,34L}$, $N_{chg/h}$

Output:
$Action \in \{allocationChange, noChange\}$

1: **Initialize:**
2: $h, t^{@}_{ETA,34L} \leftarrow t_{ETA,ac_n}$
3: $N_{\xi,34L} \leftarrow cntAc34L(t^{@}_{ETA,34L}, \xi)$
4: $Tgt \leftarrow TargetGroup(ac_n)$ ▷ The target is G1 or G2
5: **if** $N_{\xi,34L} > N_{max/\xi,34L}$ **then**
6: **if** $N_{h,34LtoR} < N_{chg/h}$ **and** $Tgt = G2$ **then**
7: $Action \leftarrow allocationChange$
8: $N_{h,34LtoR} \leftarrow N_{h,34LtoR} + 1$
9: **else**
10: $Action \leftarrow noChange$
11: **else**
12: **if** $N_{h,34RtoL} < N_{chg/h}$ **and** $Tgt = G1$ **then**
13: $Action \leftarrow allocationChange$
14: $N_{h,34RtoL} \leftarrow N_{h,34RtoL} + 1$
15: **else**
16: $Action \leftarrow noChange$
return $Action$

is an arrival-only runway, could increase departure waiting times on runway 34R. Therefore, Algorithm 1 introduces the third parameter, $N_{chg/h}$, which limits the maximum number of runway reassignments working in lines 6 and 12. On the basis of these three parameters, Sections IV-A, IV-B, and IV-C show an example of parameter setting.

A. OPTIMAL TIME FRAME FOR ARRIVAL SLOTS ON RUNWAY 34L

The parameter ξ, the time interval assigned to count the arrival aircraft (slots on the runway), is set at 10 min. The less the ξ, the more accurate the ETA required to strictly follow the sequence (i.e., two to three aircraft per 5 min). In terms of arrival traffic, the maximum time when the aircraft flies along with the sequencing leg of the PM is ∼10 min in TACA. If an aircraft is held up for more than 10 min, it will be further delayed in accordance with the aircraft holding procedure. Therefore, the time interval of 10 min serves as an indicator to detect the overflowed aircraft in the sequencing leg. After fixing ξ, the maximum arrival rate at runway 34L per hour $(N_{max/h,34L})$ is estimated to set $N_{max/\xi,34L}$ in the following section.

B. STOCHASTIC ESTIMATION OF MAXIMUM ARRIVAL RATE AT RUNWAY 34L

$N_{max/h,34L}$ has already been determined using the statistics of aircraft types, stochastic distributions of inter-aircraft time and ROT, and levels of the automation systems that supported ATCos' separation work (see [40] for detailed methodology).

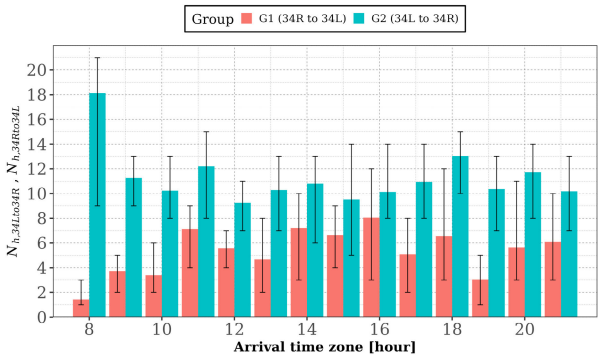

FIGURE 7. The average number of target flights, G1 and G2, defined in Fig. 6 by hour. The error bar indicates the min–max range of the value.

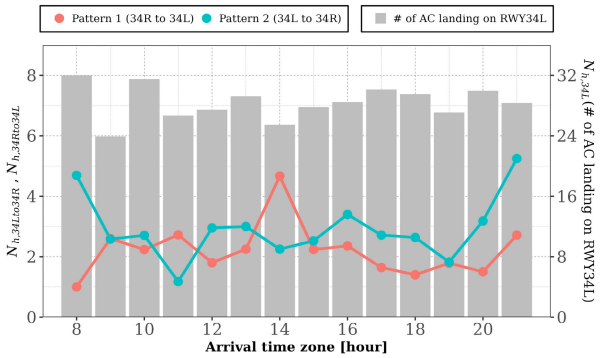

FIGURE 8. The average number of flights assigned to another runway, by hour, according to the northerly wind operation. The left vertical axis is the number of the reassignments for blue and red lines and the right vertical axis is the number of the aircraft landing on runway 34L, which is depicted as gray bars.

The current RJTT operation applies wake turbulence separation minima under the ICAO standards [41] to AMAN; hence, a maximum of 32 arrivals per hour are allowed. Furthermore, applying the new wake turbulence category, called RECAT [42], allows four more arrivals while maintaining the same automation support level. Thus, 32-36 aircraft per hour would be suitable to set the parameter $N_{max/\xi,34L}$ on an hour scale. Therefore, the optimal parameter range of $N_{max/\xi,34L}$ is 5.3-6 ($\approx$ 32-36 aircraft per hour divided by 10 min). However, only integer values can be handled to determine the frame of the sequence; thus, $N_{max/\xi,34L} = \{5, 6\}$. In the case of $N_{max/\xi,34L} = 5$, the condition to prevent aircraft overflow is conservative, causing the loss of the 34L runway slot. Furthermore, this condition triggers frequent changes in runway assignment, increasing the task volumes of approach controllers. Therefore, this study adopts $N_{max/\xi,34L} = 6$. Basically, the flow rate of runway 34L should be managed on the basis of parameters ξ and $N_{max/\xi,34L}$. However, excessive reassignment will adversely affect the departing aircraft because of the imbalance between runways 34L and 34R as well as an increase in the approach controller's task volumes. Therefore, the third parameter, $N_{chg/h}$, is used to limit the number of reassignments.

C. ANALYSIS OF CURRENT RUNWAY REASSIGNMENT

Fig. 7 shows the average numbers of G1 and G2 defined in Fig. 6 between 08:00 and 21:00, congested period in the daytime. Except at 8:00, which is the most congested period, the average number of flights in G2 is approximately 10 per hour. Meanwhile, the average number of G1 aircraft is 4–8, less than that of G2 at any time of the day. When all G1 is assigned to 34L and all G2 is assigned to 34R, the arrival rate, especially on runway 34R, will exceed the current rate, affording a lower takeoff rate on runways 05 and 34R. Therefore, constraints are needed to avoid runway imbalance, hence the importance of the third parameter of Algorithm 1.

Fig. 8 shows the hourly number of runway reassignments between 08:00 and 21:00. Notably, this change in runway assignment does not occur routinely and is independent of the G1 or G2, shown in Fig. 7. The data indicate that two to three aircraft are reassigned to other runways in an hour (red and blue dots in the figure). Therefore, according to the analysis considering ATCos' acceptable rate of the runway reassignment in an hour, the parameter $N_{chg/h}$ is estimated at 3. After designing the runway assignment rule, the speed control rule is designed in the next subsection.

V. ANALYZING OPTIMAL SPEED CONTROL RULES

Combining simulation-based optimization and data exploration techniques, speed control rules are optimally designed for the southbound traffic targeting RJTT. The speed control is implemented by ATCos at T25/24 and T14 in Fig. 3, offering each optimal rule. However, conventional studies [33], [34], [35], [36] have not designed the speed control algorithm on the basis of the traffic flow characteristics of T25/24 and T14. In other words, the foundation of the IF–THEN rule (e.g., Algorithm 1) is not solid. Therefore, the data exploration technique combining multi-objective air traffic optimization [43] and decision tree analysis [44] is utilized herein. First, a database of ideal traffic flows with speed control in en route airspace is created through multi-objective optimization. Next, the knowledge (e.g., indicators and rules contributing to speed control) in each sector is extracted from the database using decision tree analysis. Finally, the obtained knowledge is compiled into operationally feasible rules.

A. DATABASE CONSTRUCTOR: SIMULATION-BASED MULTI-OBJECTIVE OPTIMIZATION USING CELLULAR AUTOMATON-BASED MODEL

1) METHOD

Multi-objective optimization combining NSGA-II [45] and cellular automaton-based air traffic model [43] is performed to obtain suboptimal speed control solutions. The main purpose of cruise speed control is to reduce the congestion in terminal maneuvering airspace. However, there is a concern that deceleration instructions may extend the overall flight time, worsening punctuality. In addition, pop-up flights are known to have an important impact on cruise aircraft, especially when combining at merging points [46]. Therefore,

TABLE 4. The parameter setting used in (2) and (3).

Parameter	Definition
N_{PU}	The number of aircraft per day coming from the south direction with takeoff start (pop-up flights)
N_{CR}	The number of aircraft per day coming from the south direction with cruise start (cruise-inflow flights)
$T_{AA_{ac_i}}$	The actual time of arrival (arrival time at the runway) of aircraft ac_i
$T_{AD_{ac_i}}$	The actual time of departure (departure time at the origin) of aircraft ac_i

the objective functions minimize the average flight time of (1) pop-up flights from the south direction (aircraft departing from the blue dots excluding RJTT in Fig. 3) and (2) cruise-inflow flights from the south direction. The expression is formulated using the definitions of the following parameters shown in Table 4.

$$\text{minimize } f_1 = \frac{1}{N_{PU}} \sum_{i=1}^{N_{PU}} (T_{AA_{ac_i}} - T_{AD_{ac_i}}) \tag{2}$$

$$\text{minimize } f_2 = \frac{1}{N_{CR}} \sum_{i=1}^{N_{CR}} (T_{AA_{ac_i}} - T_{AD_{ac_i}}) \tag{3}$$

The design variable x_i is the deceleration speed value at the true airspeed of each arriving aircraft $ac_i (i = 0, 1, \cdots, 431)$ in the cruising state from the south at the straight line distance of 150 NM from RJTT (see Fig. 3). x_i decelerates the aircraft in each cruising state, affecting the average flight times f_1 and f_2. The constraint condition is not set to obtain the ideal traffic flow achieved by deceleration. The detailed parameter setting was already demonstrated in literature [43]. The population size and total number of evaluations are set to 500 and 200,000, respectively, which are higher than those in [43] to ensure that the solutions converge sufficiently. The range of deceleration speed, which is a design variable, allows a maximum of ∼15% [47], [48] of the true airspeed of ∼450–500 kt in the cruising state. Therefore, the values of the design variables x_i are 0, 17, 34, 51, and 68 kt corresponding to the airspeed (IAS) indicated by 0, 10, 20, 30, and 40 kt assuming the international standard atmosphere (ISA) at FL350, which is the average flight level of the speed control target. Acceleration and deceleration must be restricted with respect to the aerodynamic characteristics and structural restrictions of the aircraft. However, BADA [49] has a maximum acceleration and deceleration of 2 [ft / s ^{2}] for commercial aircraft regardless of the model. This study applies 1 [ft / s ^{2}], which is 50% of the maximum value.

2) RESULT

Fig. 9 shows the distribution of nondominated solutions in the objective function space in a two-dimensional scatter plot. As shown in Fig. 9, we obtained nondominated solutions that are superior to the original one. This result suggests that proper cruise speed control could considerably improve the overall flight time. Compared with the original solution, the

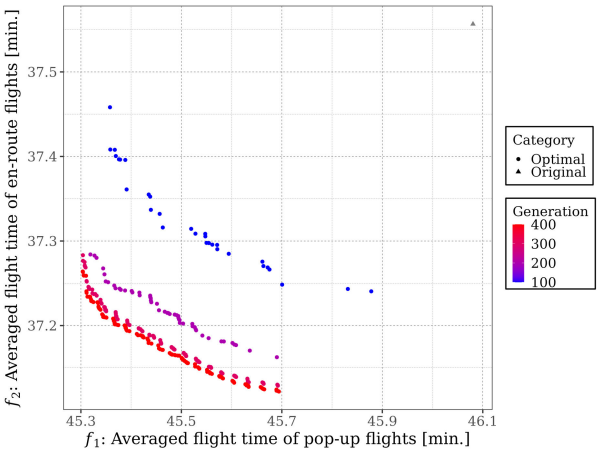

FIGURE 9. Scatter plot of objective functions f_1 and f_2 defined by (2) and (3), respectively. The horizontal axis represents the average flight time of all cruise flights (f_2), whereas the vertical axis represents the average flight time of all pop-up flights (f_1). The gray triangle is the original solution without speed control. The circles color-coded according to the number of generations from blue to red represent the cumulative nondominated solution for every 100 generations. The cumulative number of nondominated solutions obtained up to the final generation is 131.

overall flight time of the cruise and pop-up flights is reduced by the maximum average of 0.4 min (24 s) and 0.8 min (48 s), respectively.

This study finds and analyzes strategies that minimize f_2 in (2) using Pearson's correlation coefficient r [50] to measure the similarity of nondominated solutions and the solution that minimizes f_2. Herein, the minimum solution of f_2, which has a relatively large aircraft number, is selected as the criterion defined as $\boldsymbol{x}^* \in \mathbb{R}^N$, including each component x_i^*. Using the other solution $\boldsymbol{x} \in \mathbb{R}^N$ and its every component x_i, the similarity r is calculated as follows.

$$r = \frac{\sum_{i=1}^{N}(x_i^* - \mathrm{E}[\boldsymbol{x}^*])(x_i - \mathrm{E}[\boldsymbol{x}])}{\sqrt{\sum_{i=1}^{N}(x_i^* - \mathrm{E}[\boldsymbol{x}^*])^2}\sqrt{\sum_{i=1}^{N}(x_i - \mathrm{E}[\boldsymbol{x}])^2}}. \tag{4}$$

This study uses $\boldsymbol{x}^*$ and all solutions $\boldsymbol{x}$ with r exceeding 0.95. However, instead of using them as integers, each component x_i^* or x_i is converted into a binary value. When each component x_i^* or x_i is more than 0, it will be converted to 1. Here, 0 represents an aircraft maintaining its cruising speed, whereas 1 represents an aircraft decelerated by speed control. These are used as objective variable values (class labels) of decision tree analysis.

B. RULE EXTRACTION: DATA EXPLORATION VIA DECISION TREE ANALYSIS

1) METHOD

Decision tree analysis is conducted using the dataset obtained in Sec. V-A to extract the trends and characteristics of the optimal speed control strategy. The two decision trees for clusters 1 and 2 shown in Fig. 3 correspond to the sectors where the ATCos are in charge of speed control.

TABLE 5. Description of feature *F*.

Feature	Description
FlightCategory	0: pop-up flights, 1: cruise flights.
Time	The time when the decision of speed control was conducted
Alt	Altitude [ft]
GS	Ground speed [kt]
TAS	True airspeed [kt]
Wind	Wind speed in the traveling direction [kt]
RouteNum	Route ID assigned at the speed control points
DtAC_i	Distance between the aircraft and i-th aircraft ($i \leq 10$) in line in front of the aircraft [NM] (see Fig. 10)
NumAC	# of aircraft in line in front of the aircraft (see Fig. 10)

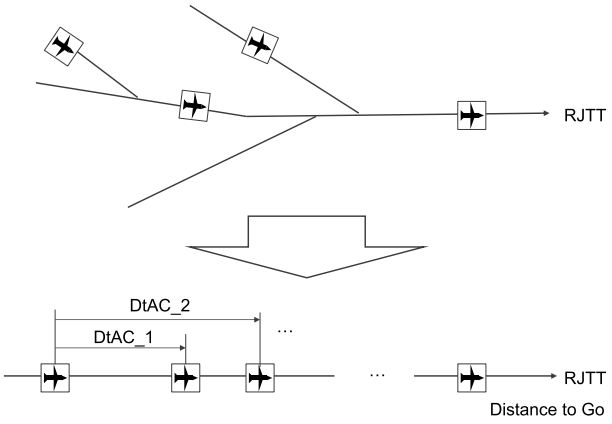

FIGURE 10. Description of DtAC_*i*. Note that DtAC_*i* is calculated by considering all the routes including clusters 1 and 2.

Target values are learned by converting the design variables of obtained nondominated solutions x_i into binary values as described in Sec. V-A. In these binary values, 0 represents the aircraft keeping nominal cruise speed, whereas 1 denotes the speed control target. The feature values F of the decision tree are local information obtained when making a decision about the speed control of each aircraft. Table 5 and Fig. 10 show the 18 features F selected to learn the speed control strategy. If the number of aircraft in front of the target is less than i corresponding to "DtAC_i," the missing values are interpolated by 99999, which is an extremely high separation value. For preprocessing, the features with correlation coefficients exceeding 0.9 are removed because of multicollinearity. The deletion method repeatedly deletes one feature that maximizes the absolute value of the correlation coefficient until the absolute value of the correlation coefficient is 0.9 or less. Features that have a large sum of absolute values of correlation coefficients with other features are selected and deleted. Consequently, "DtAC_4" to "DtAC_7" in cluster 1, "DtAC_2" to "DtAC_9" in cluster 2, and true airspeed (TAS) and wind in both clusters are deleted. For interpretability and accuracy, we divide the data into two: 70% for training and 30% for testing; set the maximum tree depth to 5, where the error is roughly 80%; and adopt the default parameters of scikit-learn in Python 3.8 as other parameters to visualize the tree.

2) RESULT

Fig. 11(a) shows a decision tree constructed using data belonging to cluster 1. The analysis focuses on the left side, where much data are classified as "SpeedReduction." As shown in Fig. 11(a), the most important features for classifying data as "SpeedReduction" are "DtAC_1" and "Alt," whose thresholds are 17.009 NM and 27350.55 ft in the first and second layer of the tree. Interestingly, the altitude threshold almost corresponds to the vertical threshold FL285 between the T24 and T25 target sectors of cluster 1 as shown in Fig 3. This result suggests that the closer the distance to the preceding aircraft when viewed on one dimension, the greater the possibility of speed control in T25, as expected. After the third layer, "DtAC_3" and "DtAC_2" are positioned as the next important features as shown in Fig. 11(a). A close observation of the distance to the third or second preceding flight suggests that a slower-speed aircraft belonging to the same cluster (speed control aircraft or pop-up flight) is approaching and slowing down. To sum up, the obtained knowledge in cluster 1 is as follows. The ATCos of T25 (FL285+) reduce the speed of flights excluding the pop-ups to the tailor inter-aircraft separation of the flights coming from the same direction before the entry fix.

Conversely, a decision tree constructed using data belonging to cluster 2 is shown in Fig. 11(b). As in Fig. 11(a), the analysis focuses on the left side, where much data are classified as "SpeedReduction." Similar to cluster 1, "DtAC_1" is the most important feature quantity for extracting the target speed control aircraft. In contrast to cluster 1, "DtAC_10" is set as the second most crucial threshold for determining the speed control target from the second layer of 11(b). "DtAC_10"$\leq$ 108.496 indicates that the distance between the aircraft subject to speed control and the 10 aircraft ahead is <108.496 NM and that 11 aircraft exist within this range on one dimension. In this situation, there is excessive congestion on the way to RJTT, which means that the aircraft subject to speed control slows down to avoid delays near the arrival airport. In the second layer and below, all nodes belonging to "DtAC_10"$\leq$ 108.496 have low Gini coefficients and are classified as "SpeedReduction." Thus, the obtained knowledge of cluster 2 is as follows. ATCos in T14 reduce the speed to smoothly merge aircraft with one from other directions, especially cluster 1, when the traffic is heavy.

C. DEVISING SPEED CONTROL RULE

Here, the distance-based features are converted to operationally feasible time-based indicators and rules on the basis of the knowledge obtained in Sec. V-B. The speed control rules for T25 and T14 are devised as shown in Algorithms 2 and 3 with the attributes listed in Tables 6 and 8, respectively. Algorithms 2 and 3 can calculate $N_{34L,\xi}$ to decide whether the speed control is necessary. If $N_{\xi,34L} > N_{max/\xi,34L}$ (line 8

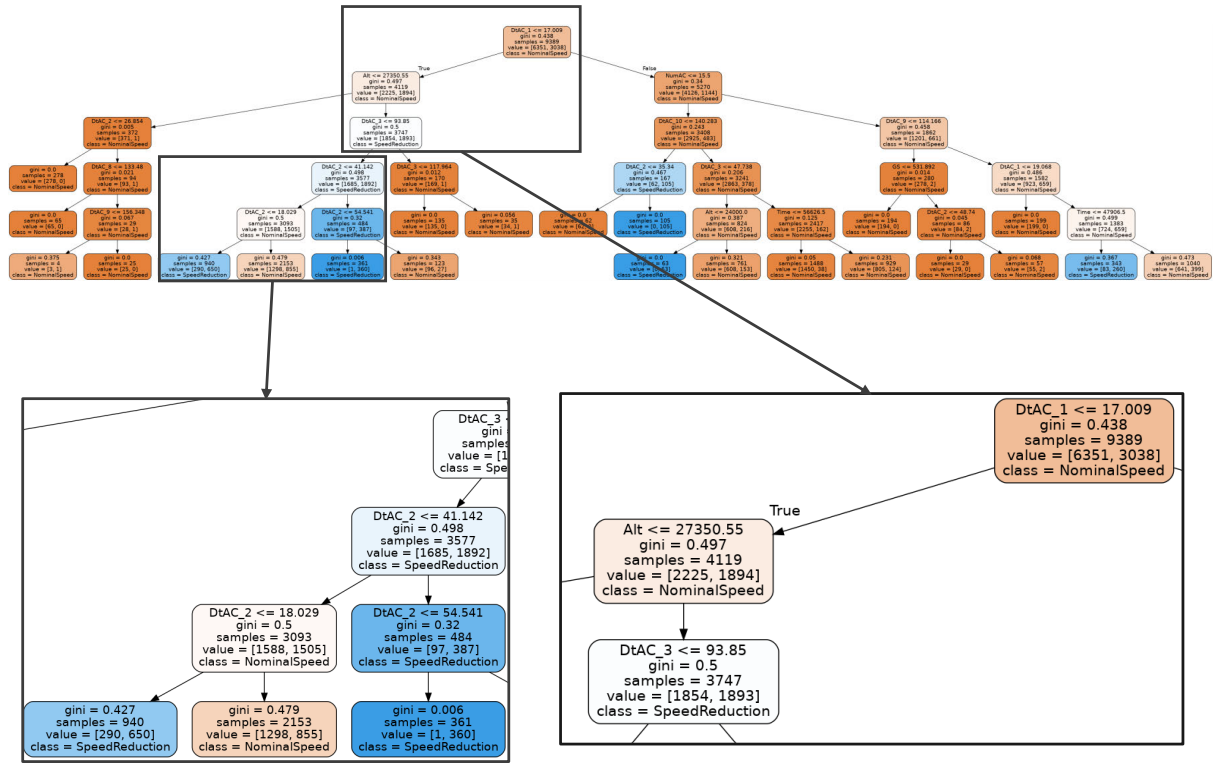

(a) Cluster 1 for ATCos, which is responsible for T24/25

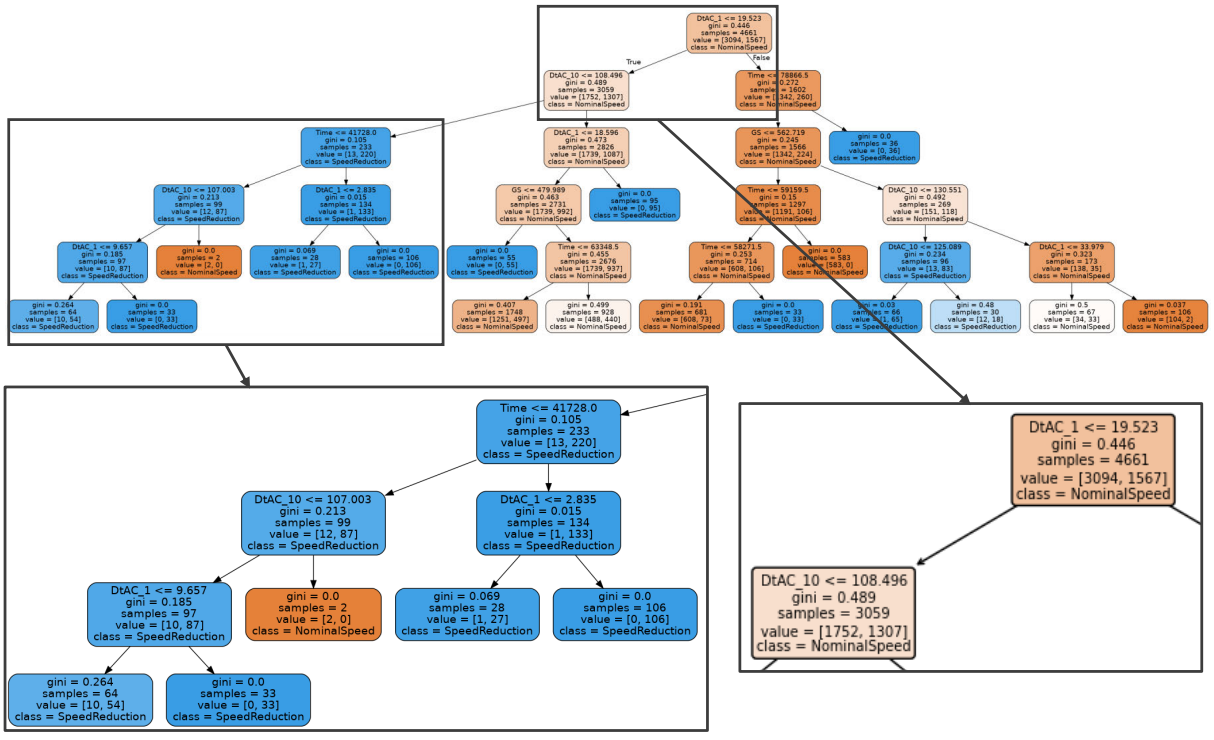

(b) Cluster 2 for ATCos, which is responsible for T14

FIGURE 11. Visualization of the decision tree. One node t has five pieces of information. (1) The feature quantity and its threshold; (2) Gini coefficient $L(t)$; (3) amount of data belonging to node t; (4) amount of data listed in (3), where the number on the right is the speed control target and that on the left is the rest; and (5) class label determined by majority voting. The class label "NominalSpeed" represents a class that does not slow down, whereas the class label "SpeedReduction" represents a class with deceleration instruction. The color shown in each node indicates the shade that accounts for more than half of the samples belonging to the class "NominalSpeed" (orange) or "SpeedReduction" (blue). The smaller the degree of irregularity within a node, the darker the color of the node.

TABLE 6. List of symbols and descriptions: Algorithm 2.

Symbol	Description
$t_{ETA@34L,ac_i}$	Set: the estimated time of arrival (ETA) of arrival sequence (AC) $(ac_1, ac_2, \cdots, ac_n, \forall i \in \{1, n\})$ at RWY34L at decision time t
$t_{ETA@SPENS,ac_i}$	Set: ETA of arrival sequence (AC) $(ac_1, ac_2, \cdots, ac_n, \forall i \in \{1, n\})$ at SPENS at decision time t
ξ	Parameter: the time frame assigned to count arrival aircraft (slots at the runway).
$N_{max/\xi,34L}$	Parameter: maximum arrival slots in time frame ξ.
$\tau 1_{cl1}$	Parameter: time interval between ETAs of decision target and preceding aircraft.
$\tau 2_{cl1}$	Parameter: time interval between ETAs of decision target and aircraft before 2nd preceding aircraft.
$t^{@}_{ETA,34L}$	Variable: ETA of the target arrival aircraft at RWY34L, which just cross over FIX_i.
$N_{\xi,34L}$	Variable: arrival aircraft numbers satisfying $[t^{@}_{ETA,34L} - \xi, t^{@}_{ETA,34L}] \in t_{ETA,ac_i}$.
$t^{@}_{ETA,SPENS}$	Variable: ETA of the target arrival aircraft ac_i at SPENS at decision time t.
$t^{p}_{ETA,SPENS}$	Variable: ETA of the aircraft preceding the target arrival aircraft ac_i at SPENS at decision time t.
$\tau 1@$	Inter-aircraft time space at SPENS between the target arrival aircraft and the preceding aircraft.
$t^{2p}_{ETA,SPENS}$	Variable: ETA of the 2nd aircraft preceding the target arrival aircraft ac_i at SPENS at decision time t.
$\tau 2@$	Variable: Inter-aircraft time space at SPENS between the target arrival aircraft and the 2nd preceding aircraft.

in Algorithms 2 and 3), these algorithms are linked to the runway assignment rules as described in Algorithm 1.

1) SPEED CONTROL RULE FOR T25

En Route AMAN supporting ATCos responsible for T25 calculates inter-aircraft time spacing at SPENS corresponding to the entry fix for cluster 1 ($\tau 1@$ and $\tau 2@$) using $t_{ETA@SPENS,ac_n}$ (target arrival) through $t_{ETA@SPENS,ac_{n-2}}$ as shown in lines 4 and 5 in Algorithm 2. When $\tau 1@$ is lower than the parameter $\tau 1_{cl1}$ and $\tau 2@$ is lower than the parameter $\tau 2_{cl1}$, ATCos are advised to reduce the cruise speed of target arrival (see line 6 in Algorithm 2). Parameters $\tau 1_{cl1}$ and $\tau 2_{cl1}$ serve as the functions that minimize the variance in the inter-aircraft spacing, including pop-up flights coming from RJOO and RJBB. This speed control targeting inter-aircraft spacing at SPENS will reduce the congestion caused by vectoring outside and inside TACA.

To find the optimal ranges of $\tau 1_{cl1}$ and $\tau 2_{cl1}$, the metrics $\tau 1@$ and $\tau 2@$ for cluster 1 are calculated using $t_{ETA@SPENS,ac_i}$ in suboptimal solution database obtained in Sec. V-A and analyzed in Sec. V-B. $t_{ETA@SPENS,ac_i}$ is calculated in our model using the decision time of speed control for ac_i (t_{ctrl,ac_i}) and the average flight time to SPENS for each airway ($\bar{T}_{SPENS,aw_j}$) used as a reference as follows.

$$t_{ETA@SPENS,ac_i} = t_{ctrl,ac_i} + \bar{T}_{SPENS,aw_j}. \tag{5}$$

Algorithm 2 En Route AMAN Speed Control Rule for ATCos of T25 (cluster 1's Passing sector) as Described in Fig. 3

Input:
$t_{ETA@34L,ac_i}$ $(\forall i \in \{1, n\})$, ▷ decision target is ac_n.
$t_{ETA@SPENS,ac_i}$ $(\forall i \in \{1, n\})$, ▷ decision target is ac_n.
ξ, $N_{max/h,34L}$, $\tau 1_{cl1}$, $\tau 2_{cl1}$

Output:
$Action \in \{reduceSpeed, noControl\}$

1: **Initialize:**
2: $t^{@}_{ETA,34L} \leftarrow t_{ETA,ac_n}$
$t^{@}_{ETA,SPENS} \leftarrow t_{ETA@SPENS,ac_n}$
$t^{p}_{ETA,SPENS} \leftarrow t_{ETA@SPENS,ac_{n-1}}$
$t^{2p}_{ETA,SPENS} \leftarrow t_{ETA@SPENS,ac_{n-2}}$
3: $N_{\xi,34L} \leftarrow cntAc34L(t^{@}_{ETA,34L}, \xi)$
4: $\tau 1@ \leftarrow t^{p}_{ETA,SPENS} - t^{@}_{ETA,SPENS}$
5: $\tau 2@ \leftarrow t^{2p}_{ETA,SPENS} - t^{@}_{ETA,SPENS}$
6: **if** $N_{\xi,34L} \leq N_{max/\xi,34L}$ **and** $\tau 1@ < \tau 1_{cl1}$ **and** $\tau 2@ < \tau 2_{cl1}$ **then**
7: $Action \leftarrow reduceSpeed$
8: **else**
9: $Action \leftarrow noControl$
return $Action$

TABLE 7. The percentile of the optimal parameter ranges for speed control of the flights in cluster 1 (DtAC_1 ≤ 17.009 ∧ Alt≥ 27350.55 in Fig 11(a)).

Parameter	0%	5%	25%	50%	75%	95%	100%
$\tau 1@$	1	3	39	80	118	451	728
$\tau 2@$	6	80	138	236	374	787	1127

Then, focusing on the flights that belong to cluster 1, we analyze the distribution of $\tau 1@$ and $\tau 2@$. Notably, the dataset contains ambiguities because it is based on simulated data.

Fig. 12 and Table 7 summarize the distribution of $\tau 1@$ and $\tau 2@$. The results show that more than 75% of $\tau 1@$ values are below 120 s and more than 50% of $\tau 2@$ values are below 240 s, corresponding approximately to the required time separation at SPENS, whereas the peaks of the distribution are located within this range. This result suggests that speed control tends to be implemented when an approximate 2-min interval is unavailable for two preceding aircraft.

2) SPEED CONTROL RULE FOR T14

En Route AMAN supporting ATCos responsible for T14 calculates the inter-aircraft time spacing on runway 34L ($\tau 1@$) and the number of arrivals per 20 min ($N_{20min,34L}$) using the ETA list on the runway $t_{ETA@34L,ac_i}$ as shown in lines 4 and 5 of Algorithm 3. When $\tau 1@$ is lower than the parameter $\tau 1_{cl2}$ and $N_{20min,34L}$ exceeds the parameter $N_{max/20min,34L,cl2}$, ATCos are advised to reduce the cruise speed of target arrival (see line 6 in Algorithm 3). The parameter $\tau 1_{cl2}$ serves as a function that reduces the variance in the inter-aircraft spacing as well as the parameter $\tau 1_{cl1}$ used in

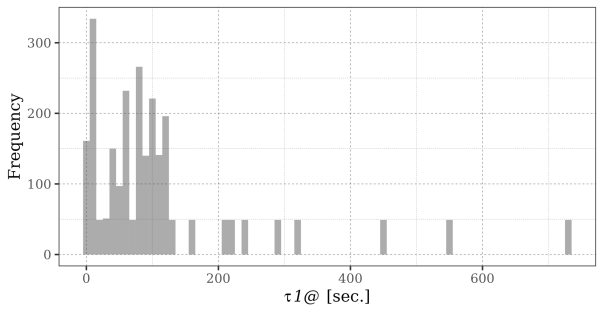

(a) $\tau 1@$

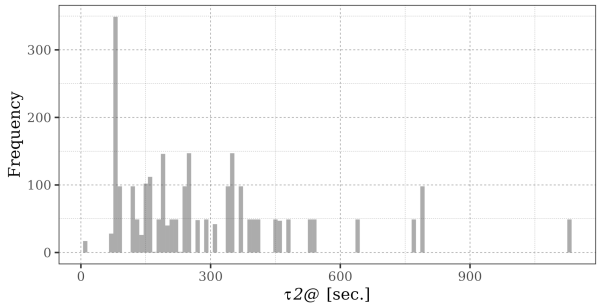

(b) $\tau 2@$

FIGURE 12. Optimal parameter ranges for speed control of the flights in cluster 1 (DtAC_1 ≤ 17.009 ∧ Alt≥ 27350.55 in Fig 11(a)).

TABLE 8. List of symbols and descriptions: Algorithm 3.

Symbol	Description
$t_{ETA@34L,ac_i}$	Set: estimated time of arrival (ETA) of arrival sequence (AC) $(ac_1, ac_2, \cdots, ac_n, \forall i \in \{1, n\})$ at RWY34L at decision time t
ξ	Parameter: the time frame assigned to count arrival aircraft (slots at the runway).
$N_{max/\xi,34L}$	Parameter: maximum arrival slots in time frame ξ.
$\tau 1_{cl2}$	Parameter: time interval between ETAs of decision target and preceding aircraft.
$N_{max/20min,34L,cl2}$	Parameter: congestion at RWY34L in time window 20 min.
$t^{@}_{ETA,34L}$	Variable: ETA of the target arrival aircraft at RWY34L, which just cross over FIX_i.
$N_{\xi,34L}$	Variable: arrival aircraft numbers satisfying $[t^{@}_{ETA,34L} - \xi, t^{@}_{ETA,34L}] \in t_{ETA,ac_i}$.
$t^{p}_{ETA,34L}$	Variable: ETA of the aircraft preceding the target arrival aircraft ac_i at RWY34L at decision time t.
$\tau 1@$	Variable: Inter-aircraft time space at RWY34L between the target arrival aircraft and the preceding aircraft.
$N_{20min,34L}$	Variable: the number of ACs scheduled to land on RWY34L in $[t_{ETA,l34L@} - 20min., t_{ETA,l34L@}]$.

Algorithm 2. The parameter $N_{max/20min,34L,cl2}$ comes from "DtAC_10"≤ 108.496 observed in Fig. 11(b), indicating congestion on runway 34L. The arrival time interval at runway 34L is assumed to be 2 min, so the feature "DtAC_10" is estimated to be 20 min as the congestion indicator. To find the optimal range of $\tau 1_{cl2}$ and $N_{max/20min,34L,cl2}$, the metrics $\tau 1@$ and $N_{34L,20\ min}$ are calculated by leveraging

Algorithm 3 En Route AMAN Speed Control Rule for ATCos of T14 (cluster 2's Passing sector) as Described in Fig. 3

Input:

$t_{ETA@RWY,ac_i}$ $(\forall i \in \{1, n\})$, ▷ decision target is ac_n.
$\xi, N_{max/h,34L}, \tau 1_{cl2}, N_{max/20min,34L,cl2}$

Output:

$Action \in \{speedReduction, noControl\}$

Initialize:
$t^{@}_{ETA,34L} \leftarrow t_{ETA,ac_n}$
$t^{p}_{ETA,34L@} \leftarrow t_{ETA,ac_{n-1}}$
$N_{34L,\xi} \leftarrow cntAc34L(t_{ETA,34L@}, \xi)$
$N_{34L,20\ min} \leftarrow cntAc34L(t_{ETA,34L@})$
$\tau 1@ \leftarrow t^{p}_{ETA,34L} - t^{@}_{ETA,34L}$
if $N_{\xi,34L} \leq N_{max/\xi,34L}$ **and** $\tau 1@ < \tau 1_{cl2}$ **and** $N_{20min,34L} > N_{max/20min,34L,cl2}$ **then**
  $Action \leftarrow speedReduction$
else
  $Action \leftarrow noControl$
return $Action$

TABLE 9. The percentile of the optimal parameter ranges for speed control for the flights in cluster 2 (DtAC_1 ≤ 19.523 ∧ DtAC_10 ≤ 108.496 in Fig 11(b)).

Parameter	0%	5%	25%	50%	75%	95%	100%
$\tau 1@$	4	6	26	43	59	102	129
$N_{20min,34L}$	11	11	11	12	14	15	15

$t_{ETA@RWY,ac_i}$ in the suboptimal solution database obtained in Sec. V-A and analyzed in Sec. V-B. $t_{ETA@RWY,ac_i}$ is calculated in our simulator using the speed control time for ac_i (t_{ctrl,ac_i}), flight time from the speed control point to the entry fixes (T_{entry,ac_i}), and average flight time in the TACA for each airway ($\bar{T}_{TACA,aw_j}$) used as a reference as follows:

$$t_{ETA@RWY,ac_i} = t_{ctrl,ac_i} + T_{entry,ac_i} + \bar{T}_{TACA,aw_j}. \quad (6)$$

Then, the distribution analysis of $\tau 1@$ and $N_{34L,20\ min}$ focuses on the flights that belong to cluster 2.

Fig. 12 and Table 9 summarize the distribution of $\tau 1@$ and $N_{34L,20\ min}$. The results show that more than 75% of $\tau 1@$ values are below 60 s, corresponding to approximately the required time separation at runway 34L, whereas the peaks of the distribution are located at 40 s. Although there is some variation depending on the design variables $x_i \in 17, 34, 51, 68[kt]$, the deceleration effect generally leads to ∼1-2-min extension, which is considered to create the 2-min interval on runway 34L. Furthermore, $N_{20min,34L}$ values are distributed between 11 and 15 and near the maximum hourly runway 34L arrival rate. This result suggests that speed control tends to be implemented when runway 34L is expected to be congested. When used in combination with the runway assignment rule based on Algorithm 1, this parameter close to $N_{max/\xi,34L} = 6$ ($\xi = 10$ min.) is not always necessary because these flights are reassigned to runway 34R.

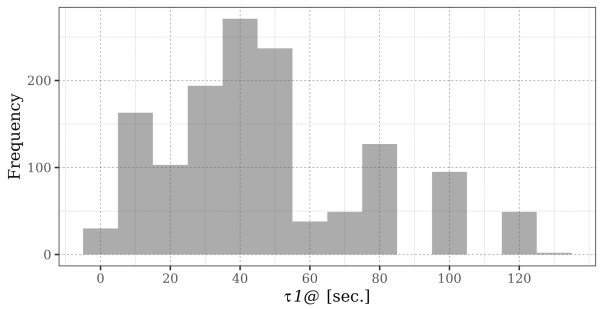

(a) $\tau 1@$

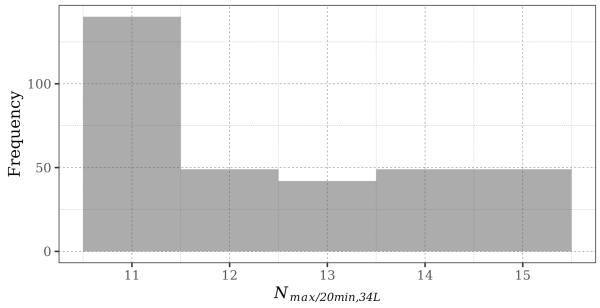

(b) $N_{20min,34L}$

FIGURE 13. Optimal parameter ranges for speed control of the flights in cluster 2 (DtAC_1 ≤ 19.523 ∧ DtAC_10 ≤ 108.496 in Fig 11(b)).

VI. VALIDATION VIA 4D-TRAJECTORY- AND AGENT-BASED SIMULATION

A. BACKGROUND OF SIMULATION

In previous sections, our proposed En Route AMAN equipped with Algorithms 1, 2, and 3 was devised through stochastic approach and data exploration technique. However, it was devised without considering the characteristics of the traffic flow on the ground surface and the sequencing and spacing of the terminal areas; actual operation by ATCos was not explicitly regarded. Thus, this study finally conducts trajectory-based simulation covering both airspace and surface with the ATC rules to demonstrate that the devised En Route AMAN functions as intended.

B. SIMULATION ENVIRONMENT

AirTOP software [51], an agent-based simulator, is used for validation following the literature [36], [40]. This study simulates gate-to-gate traffic flow that comprises departures at RJTT arriving at the end of runway thresholds and arrivals at RJTT coming from en route airspace to the gates. A detailed simulation environment for en route traffic was already clarified in [40] and [36], including separation rules and weather conditions. Therefore, this study additionally demonstrates the runway interaction between arrivals and departures and the environment of surface traffic.

1) SEPARATION RULES BETWEEN ARRIVALS AND DEPARTURES

On the departure/arrival mixed-mode runway, that is, runway 34R in RJTT, a departing aircraft cannot take off when an arriving one approaches 3.5 NM from the runway threshold. This takeoff aircraft that misses departure will take off as soon as the separation [41] is ensured after the relevant arriving aircraft has vacated the runway. On the departure/arrival crossed-mode runway, that is, runway 05 in RJTT, the departing aircraft takes off immediately after the arriving one on runway 34R has cleared the takeoff course from runway 05. On runways 34R and 05, departure–departure pairs follow the wake turbulence minimum separation [41].

2) TAXIWAY AND GROUND INTERACTION RULE

The taxiways, aprons/ramps, gates, and terminal buildings as well as the geometrical and operational restrictions on the surface and in the surrounding airspace are airport-specific factors that affect the characteristics of air traffic, being thereby modeled in our simulator as shown in Fig. 5. Each aircraft chooses the route that minimizes the cost of passage that we adjust in the simulation, resulting in most aircraft taking the path close to the actual operation. The speed is set at a fixed value for each model, and there is no variation in speed from pilot to pilot or owing to congestion, which exists in reality. For runway crossings, the aircraft stops when an arrival approaches within 3.5 NM from runway threshold and crosses immediately after another one is landed.

3) CONFIGURATION OF RUNWAY ASSIGNMENT AND SPEED CONTROL RULES

The runway assignment and speed control rules work at the moment of passing 180 NM away from the waypoint named XAC (∼230 NM away from RJTT; see literature [36]) for southbound traffic and 120 NM from RJTT for northbound traffic. The runway assignment parameters used in Algorithm 1, ξ, $N_{max/\xi,34L}$, and $N_{chg/h}$, are set to 10 min, 6 aircraft per ξ, and 3, respectively. Following these values, the target flights of G1 and G2 are reassigned to runways 34L and 34R, respectively, on the basis of the northerly wind operation in which southbound and northbound traffic land on runways 34L and 34R, respectively. The speed control parameters used in Algorithms 2 and 3, $\tau 1_{cl1}$, $\tau 2_{cl1}$, and $\tau 1_{cl2}$ are set to 80, 236, and 43 s, corresponding to the median values of Tables 7 and 9. $N_{max/20min,34L,cl2}$ is set to 8, considering the runway reassignment effect. Then, the flights categorized into the speed control are instructed to reduce IAS by 20 kt that any aircraft can decelerate, which has the time adjustment effect of ∼1–2 min in the cruise section. Finally, the metrics compared with these parameters are calculated using (5) and (6).

C. VALIDATION RESULTS

Returning to the question posed at the beginning of this study, we show the effectiveness of the devised rules by comparing them with the northerly wind operation, which does not implement runway reassignment and speed control, through

TABLE 10. The numbers of aircraft applying for runway reassignment and speed control for 20 d in AirTOP simulation. $N_{h,ctrl/cl1}$ and $N_{h,ctrl/cl2}$ are the speed control aircraft numbers in clusters 1 and 2 using Algorithms 2 and 3, respectively.

h	Algorithm 1		Algorithm 2	Algorithm 3
	$N_{h,34RtoL}$	$N_{h,34LtoR}$	$N_{h,ctrl/cl1}$	$N_{h,ctrl/cl2}$
6	0.30	0.00	0.15	0.00
7	0.80	0.00	0.10	0.00
8	0.15	3.00	3.75	0.85
9	2.80	2.05	1.10	1.00
10	1.95	2.25	2.90	0.80
11	3.00	2.10	2.40	0.55
12	2.80	2.20	0.95	1.00
13	2.55	2.50	1.00	1.20
14	3.00	1.50	2.20	0.75
15	2.95	2.00	1.40	1.35
16	2.95	2.20	2.00	1.15
17	2.55	2.50	1.20	1.15
18	2.55	2.80	2.20	1.50
19	1.85	2.55	1.95	1.10
20	2.85	2.85	1.35	1.10
21	2.25	2.90	1.55	0.85
22	1.80	1.35	0.60	0.50
TTL.	37.10	34.75	26.80	14.85

scenario-based simulation. First, we conduct the simulation of the northerly wind operation as the baseline, which is treated as the ''Before Control'' denoted as ''BEF.'' After the simulation, the metrics used to apply the devised rules are calculated using the obtained result of ''BEF.'' Accordingly, we conduct the simulation according to the scenario created by the devised rules, which is treated as the ''After Control'' denoted as ''AFT.''

1) NUMBERS OF AIRCRAFT APPLYING FOR RUNWAY REASSIGNMENT AND SPEED CONTROL

Table 10 presents the reflection of the number of aircraft applying for runway reassignment and speed control in Algorithms 1 to 3. The total $N_{h,34RtoL}$, including both clusters 1 and 2, is 37.10, equivalent to the sum of $N_{h,ctrl/cl1}$ and $N_{h,ctrl/cl2}$, which is 41.65. This indicates that the runway reassignment and speed control can function almost equally well. Furthermore, between 8:00 and 21:00, $N_{h,34RtoL}$ and $N_{h,34LtoR}$ remain roughly between 2 and 3, indicating that parameter $N_{chg/h}$ set to 3 maintains the demand–capacity balance at runways 34L and 34R as intended. In particular, at 8:00, the peak hour for southbound traffic, there is an imbalance of 0.15 for $N_{h,34RtoL}$ and 3 for $N_{h,34LtoR}$. The value of $N_{h,ctrl/cl1}$ (3.75) is also the largest, suggesting that the inter-aircraft spacing is tight. Thereafter, $N_{h,34RtoL}$ is larger than $N_{h,34LtoR}$ from 11:00 to 17:00, when the sourthbound traffic is not heavy. This is because of the maximum utilization of runway 34L. Accordingly, speed control coordinates the reduced inter-aircraft separation: $N_{h,ctrl/cl1}$ and $N_{h,ctrl/cl2}$ hover between 0.95 and 2.40 and between 0.55 and 1.35, respectively. Conversely, in the second peak of traffic in the southwest direction, from 18:00 to 21:00, $N_{h,34LtoR}$ again exceeds $N_{h,34RtoL}$, suggesting that Algorithm 1 tends to moderate its peak.

2) EVALUATION WITH KEY PERFORMANCE INDICATORS

To achieve the three goals mentioned in Sec. VI-A, six key performance indicators (KPIs) of our En Route AMAN are defined as follows.

- d_{TMA} is the arrival sequencing and spacing delay for arrivals at runways 34L and 34R in the terminal maneuvering area.
- TX_{arr} is the taxiing time from the runway threshold to the spot/gate of arrival flights.
- FT_{arr} is the flight time from the departure point to the runway threshold of arrival flights.
- GtG_{arr} is the gate-to-gate time corresponding to the duration from the departure point to spot/gate for arrivals.
- TX_{dep} is the taxiing time from the spot/gate to the runway threshold of departure flights.
- W_{dep} is the waiting time for departure flights at runways 05 and 34R.

The above six KPIs for a 20-d simulation with the result of the Wilcoxon signed-rank test are summarized in Table 11. For 19 pairs of the median of d_{TMA}, 20 pairs of maximum d_{TMA}, and 20 pairs of the median of TX_{arr} before and after implementing IF–THEN rules, reassigning the runways and controlling the inter-arrival times of flights considerably reduce the median of d_{TMA} and TX_{arr} distribution of population. From this test, we can conclude that the control smoothen the flow of arrivals on average. For the median of the maximum FT_{arr} distribution of population, it cannot be stated that the time can be considerably reduced by the operation, instead it should be stated that the flight time was reduced by 0.83 min (49.8 s) at most (Day 17) for three days, which remained constant for twelve days. Further, the flight time was increased by 1.14 min (68.4 s) at most (Day 9) for five days. There are several possible explanations for this result. The foremost cause of discrepancy can be the long travel from south to runway 34R as illustrated in Fig. 4, which is not considered in d_{TMA}. One possible solution is to direct the reassigned traffic to the final approach fix to runway 34R when the northbound traffic is not congested. Another possible explanation is that this reassigned traffic to runway 34R follows the in-trail separation at SPENS and SELNO in Fig. 3 even though they are not involved with sequencing and spacing at runway 34L. Therefore, a separate IAF for the reassigned traffic to runway 34R (e.g., SPENS' and SELNO') could be prepared to achieve an even smoother arrival traffic flow. Even with the extension of flight time, the effect of GtG_{arr} reduction in 13 d has been recognized, so this operation is expected to improve punctuality compared with the current situation.

For departing aircraft, TX_{dep} is considerably reduced during the 5-d period only (Days 2, 5, 13, 14, and 20), indicating that the effect of the runway reassignment is limited. However, there are no considerably worse days, and the averaged median and maximum TX_{dep} were reduced by 0.05 min (3 s) and 0.18 min (10.8 s), respectively. Accordingly, we conclude

TABLE 11. Key performance indicators (KPIs) for 20 d in AirTOP simulation. BEF is the result of northerly wind operation, whereas AFT is due to our En Route AMAN with its difference (DIF). Bold values in the rows of DIF and the columns of Q2 denote medians decreased (red) and increased (blue) at the 5% level of significance in the Wilcoxon signed-rank sum test. The last row shows the total reduction in each KPI according to the northerly wind operation (BEF) using 20-d AirTOP simulation.

i		d_{asas} [min.]		TX_{arr} [min.]		FT_{arr} [min.]		GtG_{arr} [min.]		TX_{dep} [min.]		W_{dep} [min.]	
		Q2	Max	Q2	Max	Q2	Max	Q2	Max	Q2	Max	Q2	Max
	BEF	3.43	16.17	6.43	13.88	43.23	66.67	49.77	72.22	15.32	34.22	0.03	13.07
1	AFT	2.37	12.67	6.02	13.52	42.53	67.43	49.37	72.37	15.41	33.52	0.03	11.62
	DIF	**−1.07**	−3.50	**−0.42**	−0.37	−0.70	+0.77	**−0.40**	+0.15	+0.09	−0.70	0.00	−1.45
	BEF	3.85	15.60	6.48	13.65	44.10	63.43	50.62	73.38	15.60	37.78	0.03	11.03
2	AFT	2.52	13.18	6.05	13.95	43.95	66.97	50.53	72.85	15.53	37.78	0.03	11.62
	DIF	**−1.33**	−2.42	**−0.43**	+0.30	**−0.15**	+3.53	−0.08	−0.53	**−0.07**	0.00	0.00	+0.58
	BEF	3.52	17.80	6.43	13.33	40.67	59.83	47.25	70.23	15.53	40.57	0.05	12.97
3	AFT	2.42	10.47	6.05	13.55	40.87	63.00	47.05	70.23	15.52	41.72	0.03	14.28
	DIF	**−1.10**	−7.33	**−0.38**	+0.22	+0.20	+3.17	**−0.20**	0.00	−0.02	+1.15	**−0.02**	+1.32
	BEF	2.97	15.08	6.42	14.43	40.37	62.83	47.33	70.98	15.27	41.33	0.03	10.18
4	AFT	2.08	12.47	6.02	14.07	40.80	61.45	47.20	69.30	15.25	41.33	0.03	9.03
	DIF	**−0.88**	−2.62	**−0.40**	−0.37	+0.43	−1.38	**−0.13**	−1.68	−0.02	0.00	0.00	−1.15
	BEF	2.27	16.63	6.38	13.70	40.42	65.52	47.01	73.70	15.36	39.37	0.03	10.80
5	AFT	1.55	15.63	5.94	14.05	40.74	64.37	46.99	71.80	15.41	40.42	0.03	10.85
	DIF	**−0.72**	−1.00	**−0.44**	+0.35	+0.33	−1.15	**−0.02**	−1.90	+0.05	+1.05	0.00	+0.05
	BEF	2.85	12.88	6.43	14.93	40.46	67.65	47.17	72.25	15.28	35.75	0.03	17.60
6	AFT	1.74	10.08	5.98	15.00	40.16	65.87	46.62	70.48	15.29	35.63	0.03	22.38
	DIF	**−1.11**	−2.80	**−0.45**	+0.07	−0.30	−1.78	**−0.56**	−1.77	+0.02	−0.12	0.00	+4.78
	BEF	2.59	21.03	6.60	16.52	40.59	63.20	47.15	70.97	15.25	30.03	0.03	10.12
7	AFT	1.62	19.02	6.13	15.92	40.71	61.42	47.09	69.57	14.92	29.07	0.03	10.20
	DIF	**−0.98**	−2.02	**−0.47**	−0.60	+0.12	−1.78	**−0.06**	−1.40	**−0.33**	−0.97	0.00	+0.08
	BEF	2.98	16.08	6.38	15.18	39.16	62.57	45.57	70.05	15.42	34.95	0.03	13.72
8	AFT	1.99	12.17	5.96	15.32	39.77	60.92	45.91	65.83	15.34	34.95	0.03	9.85
	DIF	**−0.99**	−3.92	**−0.42**	+0.13	**+0.61**	−1.65	+0.34	−4.22	−0.07	0.00	0.00	−3.87
	BEF	3.73	13.60	6.37	13.63	38.99	59.15	45.83	65.53	14.77	31.40	0.03	12.18
9	AFT	3.95	13.08	5.97	18.45	40.13	61.20	46.35	66.35	14.63	31.40	0.03	9.72
	DIF	+0.22	−0.52	**−0.39**	+4.82	**+1.14**	+2.05	**+0.52**	+0.82	−0.13	0.00	0.00	−2.47
	BEF	3.28	19.63	6.43	14.88	39.10	59.28	46.07	67.77	15.33	42.73	0.03	11.12
10	AFT	2.08	12.58	6.00	13.98	39.32	60.07	45.88	66.62	15.49	41.72	0.03	14.80
	DIF	**−1.20**	−7.05	**−0.43**	−0.90	+0.22	+0.78	**−0.18**	−1.15	+0.16	−1.02	0.00	+3.68
	BEF	3.92	20.10	6.43	12.43	39.77	59.73	46.38	65.15	15.13	37.53	0.03	15.38
11	AFT	2.36	13.40	6.08	13.32	39.70	59.23	46.17	67.30	15.13	35.65	0.03	16.75
	DIF	**−1.56**	−6.70	**−0.35**	+0.88	−0.07	−0.50	**−0.22**	+2.15	+0.00	−1.88	0.00	+1.37
	BEF	3.58	17.02	6.47	13.65	39.70	63.03	46.35	69.75	15.08	36.33	0.03	13.38
12	AFT	2.42	16.03	6.02	11.33	39.62	60.43	46.17	65.72	14.93	35.78	0.03	20.17
	DIF	**−1.17**	−0.98	**−0.45**	−2.32	−0.08	−2.60	**−0.18**	−4.03	−0.15	−0.55	0.00	+6.78
	BEF	3.88	13.80	6.37	14.08	39.73	60.62	46.40	67.02	15.62	32.63	0.03	17.37
13	AFT	3.70	13.08	5.98	13.82	40.47	65.13	46.88	72.00	15.29	30.78	0.03	8.27
	DIF	**−0.18**	−0.72	**−0.38**	−0.27	**+0.73**	+4.52	+0.48	+4.98	**−0.33**	−1.85	0.00	−9.10
	BEF	3.42	18.95	6.37	15.60	39.37	61.45	45.98	71.08	15.22	36.55	0.03	10.42
14	AFT	2.41	16.87	5.98	12.72	39.02	65.07	45.58	70.32	15.03	36.55	0.03	8.93
	DIF	**−1.01**	−2.08	**−0.38**	−2.88	**−0.35**	+3.62	**−0.40**	−0.77	**−0.20**	0.00	0.00	−1.48
	BEF	2.77	17.35	6.38	14.78	38.65	61.72	45.75	73.88	15.33	36.58	0.03	12.90
15	AFT	2.33	13.07	5.91	12.85	38.92	61.03	45.58	67.73	15.23	36.58	0.03	8.68
	DIF	**−0.44**	−4.28	**−0.47**	−1.93	+0.27	−0.68	**−0.17**	−6.15	−0.10	0.00	0.00	−4.22
	BEF	3.61	20.22	6.29	13.40	39.26	59.77	45.67	68.82	15.07	33.85	0.03	13.62
16	AFT	2.66	16.22	6.00	15.00	39.90	60.63	45.92	68.58	15.13	33.40	0.03	10.05
	DIF	**−0.95**	−4.00	**−0.29**	+1.60	**+0.64**	+0.87	+0.25	−0.23	+0.06	−0.45	0.00	−3.57
	BEF	4.13	20.13	6.40	14.10	39.38	58.07	46.17	70.60	15.30	30.70	0.03	10.27
17	AFT	1.73	14.30	5.98	13.33	38.55	64.38	45.32	70.68	15.28	32.62	0.03	10.47
	DIF	**−2.40**	−5.83	**−0.42**	−0.77	**−0.83**	+6.32	**−0.85**	+0.08	−0.03	+1.92	0.00	+0.20
	BEF	3.03	17.02	6.37	13.65	38.42	65.20	45.17	74.82	15.23	33.55	0.03	16.23
18	AFT	2.94	14.35	6.00	13.15	39.15	62.70	45.36	72.42	15.30	33.58	0.03	17.27
	DIF	**−0.09**	−2.67	**−0.37**	−0.50	**+0.73**	−2.50	**+0.19**	−2.40	+0.07	+0.03	0.00	+1.03
	BEF	4.28	18.40	6.38	13.72	39.23	62.50	45.97	72.17	15.52	37.68	0.03	10.88
19	AFT	3.50	15.20	5.98	14.32	39.42	61.57	46.05	68.07	15.60	37.43	0.03	13.98
	DIF	**−0.78**	−3.20	**−0.40**	+0.60	+0.18	−0.93	**+0.08**	−4.10	+0.08	−0.25	0.00	+3.10
	BEF	3.07	15.05	6.37	14.60	38.55	59.30	45.57	68.53	15.45	36.42	0.03	18.68
20	AFT	2.28	11.90	5.99	13.93	38.64	63.02	45.26	69.03	15.28	36.42	0.03	11.13
	DIF	**−0.78**	−3.15	**−0.37**	−0.67	+0.09	+3.72	**−0.31**	0.50	**−0.17**	0.00	0.00	−7.55
	BEF	3.36	17.13	6.41	14.21	39.96	62.08	46.66	70.44	15.30	36.00	0.03	13.10
AVE.	AFT	2.43	13.79	6.00	14.08	40.12	62.79	46.56	69.36	15.25	35.82	0.03	12.50
	DIF	−0.93	−3.34	−0.41	−0.13	+0.16	+0.72	−0.09	−1.08	−0.05	−0.18	0.00	−0.59
TTL.		−21.03434%		−6.925865%		+0.7639649%		−0.3290264%		−0.3989101%		−5.215513%	

that the runway reassignment has little adverse effect on the departures on the ground surface. W_{dep} has a similar trend. However, there are days when the maximum value increases at most (e.g., Days 6, 10, 12, and 19) by 6.78 min.

VII. DISCUSSION

As stated in the Introduction, our main objective was to scientifically design interpretable runway assignment and speed control strategies and rules that are operationally feasible for implementing En Route AMAN. In our contribution, we proposed the concept of en route arrival management through short-term runway flow and inter-aircraft control originating from the existing studies based on the queuing theory [33], [34], [35], [36]. We used RJTT as a case study for comparison. The optimized runway assignment rule selects the target minimizing the taxiing time when the runway flow per a time window exceeds the maximum calculated by the stochastic distribution of inter-aircraft time and ROT at runway 34L. The speed control rules are devised through simulation-based optimization and decision trees. We analyzed the airspace bottleneck and found the optimal strategy based on inter-aircraft control according to each traffic cluster of the entry fix.

The most important result of the validation fast-time simulation is that the optimized IF–THEN rule-based algorithms reduced the total arrival sequencing and spacing delay and arrival taxiing time by 21% (median: 0.93 min, i.e., 55.8 s) and 6.9% (median: 0.41 min, i.e., 24.6 s) compared with the baseline scenario. This result suggests that the rules extracted and constructed with the CA-based model reduce the delay time even in the AirTOP simulation, which explicitly considers the 4D trajectory and ATC rules. Furthermore, the obtained result corroborates our recent study [36] referred to as the benchmark, where 11.5% (half the effectiveness of this study) delay reduction was achieved using the same simulation environment via inter-aircraft control only but not considering the IAF separation constraints and runway reassignment. Therefore, the validation result obtained herein has further strengthened the hypothesis that inter-arrival control [33], [34], [35], [36] in combination with airline-oriented runway assignment effectively mitigates congestion in the airspace while reducing the taxiing time. In terms of flow control, although Schultz et al. [31] and Jun et al. [32] only focused on speed control in the distant airspace of more than 300NM from the destination, the runway flow control herein shows the potential to achieve significant delay reduction not only in the terminal maneuvering area but also on the airport surface.

Interestingly, our decision tree analysis revealed that the optimal speed control strategy varies according to the traffic cluster and substantiated the idea that the bottleneck exists in the airspace as well as runways, which are the traditional research focus [17], [18], [19], [20], [21], [22], [23], [24]. As hypothesized, especially in cluster 1 herein, where the traffic volume is high, the IAF rather than runways is the bottleneck, which suggests that it is better to manage arrivals in two stages, which is consistent with the approach of Khassiba et al. [28]. They outperformed the 73.5% cut of the total delay but assumed that the deviation condition for STA at IAF follows $N(0, \sigma^2)$ (σ=30 s, 60 s), not guaranteeing that a good-quality STA would always be obtained in a realistic amount of time. Our rule-based speed control with inter-aircraft spacing based on ETA is not truly optimal but has the advantage of providing operationally feasible advisory with computation time only for ETA calculation while showing stable delay reduction theoretically [33], [34], [35], [36] and practically herein. From the viewpoint of ATCos' task volumes, focusing on the bottleneck is more effective than performing absolute time management at every waypoint as in Jones et al. [27].

The runway reassignment rule, such as Algorithm 1 herein, is determined by selecting the target and estimating the maximum arrival rate at the target runway when the target airport changes. Conversely, the simulation-based optimization and decision tree analysis are necessary steps to determine the rule structure and parameter range (for instance, Algorithms 2 and 3 herein). Our approach requires trial and error, as we do not always obtain useful information depending on the optimization problem definition and the parameters of the data to be extracted. For Tokyo International Airport (RJTT), where speed control is assumed to be performed in the airspace in which ''metering'' operation begins, we selected features such as DtAC_i because relative spacing would be effective here rather than absolute time management due to ETA uncertainty based on a queueing model [33], [34], [35], [36]. Thus, while it is necessary to reflect the constraints based on the target with different topology and situation, the basic methodology itself is general enough to be applicable to other airspace and airports with multiple runway.

VIII. CONCLUDING REMARK

This study aimed to implement operationally feasible En Route AMAN using RJTT as a case study. Therefore, we adopted runway assignment and speed control strategies and rules to demonstrate a scientific system design of flow-based en route arrival management at large-scale airports with multiple runways. The runway assignment rule selects the target that minimizes the taxi time, helping avoid the overflow capacity at runway 34L in a time window within 10 min estimated through the stochastic distribution of the inter-aircraft time and ROT. The speed control rules were formulated through simulation-based optimization and decision tree analysis with respect to each traffic cluster of entry fix. Therefore, the optimal speed control rules were obtained to customize the inter-aircraft spacing at bottleneck waypoints according to the traffic characteristics, with a tendency for spacing to be more upstream when there is more traffic and vice versa. Finally, a fast-time simulation by AirTOP was conducted to validate the devised IF–THEN rules. The results revealed that the airline-oriented runway reassignment and speed control, employed to adjust the relative interval between aircraft, considerably reduced the median of arrival

sequencing and spacing delay and arrival taxi time by 21% (55.8 s) and 6.9% (24.6 s). Our findings showed that while maintaining the interpretability and viability of En Route AMAN implementation, even operationally feasible rules that are not really optimal schedule time of arrivals can potentially afford promising congestion mitigation.

Our main challenge is to propose a scientific and systematic approach by integrating data analysis, theoretical modeling, and simulation evaluation to design future air traffic management. Hence, our future study will improve the proposed methodology to design a better ATC system. Therefore, various simulations will be performed by changing the parameters of the rules and input data conditions while investigating the impact of departure waiting time on runways. Furthermore, we will evaluate the operational feasibility in terms of ATCos' workload by performing human-in-the-loop simulations that mimic actual ATC radar operations. To validate the universality of our approach, it will be applied to other target airspace and airports. Extending our approach will contribute to finding the optimal strategy for coordinating the arrivals with departures and surface traffic in airport operations.

ACKNOWLEDGMENT

The authors would like to thank JCAB for providing the air traffic data. In addition, the air traffic flow simulator used herein was developed in the "Exploratory Challenge 2 (hp190163) on Post-K computer."

REFERENCES

[1] *Arrival Manager—Implementation Guidelines and Lessons Learned*, EUROCONTROL, Brussels, Belgium, 2010, p. 14.
[2] *COVID-19 Outlook for Air Travel in the Next 5 Years*, IATA, Montreal, QC, Canada, May 2020.
[3] H. Erzberger and E. Itoh, "Design principles and algorithms for air traffic arrival scheduling," NASA, Washington, DC, USA, Tech. Rep., TP-2014-218302, 2014.
[4] *Concept of Operations for the Next Generation Air Transportation System Version 3.2*, Federal Aviation Admin. Joint Planning Develop. Office, Washington, DC, USA, 2010.
[5] *NextGen Portfolio—Time Based Flow Management*, Federal Aviation Administration, Washington, DC, USA, 2017.
[6] J. Thipphavong, J. Jung, H. Swenson, L. Martin, M. Lin, and J. Nguyen, "Evaluation of the terminal sequencing and spacing system for performance-based navigation arrivals," in *Proc. IEEE/AIAA 32nd Digit. Avionics Syst. Conf. (DASC)*, Oct. 2013, pp. 1A2-1–1A2-16.
[7] P. Van Tulder, "Flight deck interval management flight test final report," NASA, Washington, DC, USA, Tech. Rep., CR-2017-219626, Jun. 2017.
[8] *European ATM Master Plan Edition 2015*, Single Eur. Sky ATM Res. Joint Undertaking, Brussels, Belgium, 2015.
[9] *Cross Border SESAR Trials for Enhanced Arrival Management: Periodic Reporting for Period 1—PJ25 Xstream*, European Commission, Brussels, Belgium, 2017.
[10] International Civil Aviation Organization. (May 2018). *Long Range ATFM Concept Trials*. The Eighth Meeting of the ICAO Asia/Pacific Air Traffic Flow Management Steering Group (ATFMSG/8). [Online]. Available: https://www.icao.int/APAC/Meetings/2018
[11] *Long-Term Vision for the Future Air Traffic Systems*, Civil Aviation Bur., Tokyo, Japan, 2010.
[12] E. Itoh, M. Brown, A. Senoguchi, N. Wickramasinghe, and S. Fukushima, "Future arrival management collaborating with trajectory-based operations," in *Air Traffic Management and Systems II*. Cham, Switzerland: Springer, 2017, pp. 137–156.
[13] B. Kim, L. Li, and J.-P. Clarke, "Runway assignments that minimize terminal airspace and airport surface emissions," *J. Guid., Control, Dyn.*, vol. 37, no. 3, pp. 789–798, May 2014.
[14] P. Avella, M. Boccia, C. Mannino, and I. Vasilyev, "Time-indexed formulations for the runway scheduling problem," *Transp. Sci.*, vol. 51, no. 4, pp. 1196–1209, Nov. 2017.
[15] D. Briskorn and R. Stolletz, "Aircraft landing problems with aircraft classes," *J. Scheduling*, vol. 17, no. 1, pp. 31–45, Feb. 2014.
[16] A. Lieder, D. Briskorn, and R. Stolletz, "A dynamic programming approach for the aircraft landing problem with aircraft classes," *Eur. J. Oper. Res.*, vol. 243, no. 1, pp. 61–69, May 2015.
[17] X.-B. Hu and E. A. D. Paolo, "A ripple-spreading genetic algorithm for the aircraft sequencing problem," *Evol. Comput.*, vol. 19, no. 1, pp. 77–106, Mar. 2011.
[18] M. Ahmed, S. Alam, and M. Barlow, "A cooperative co-evolutionary optimisation model for best-fit aircraft sequence and feasible runway configuration in a multi-runway airport," *Aerospace*, vol. 5, no. 3, p. 85, Aug. 2018.
[19] A. Salehipour, M. Modarres, and L. Moslemi Naeni, "An efficient hybrid meta-heuristic for aircraft landing problem," *Comput. Oper. Res.*, vol. 40, no. 1, pp. 207–213, Jan. 2013.
[20] G. Hancerliogullari, G. Rabadi, A. H. Al-Salem, and M. Kharbeche, "Greedy algorithms and metaheuristics for a multiple runway combined arrival-departure aircraft sequencing problem," *J. Air Transp. Manage.*, vol. 32, pp. 39–48, Sep. 2013.
[21] A. Ghoniem, F. Farhadi, and M. Reihaneh, "An accelerated branch-and-price algorithm for multiple-runway aircraft sequencing problems," *Eur. J. Oper. Res.*, vol. 246, no. 1, pp. 34–43, Oct. 2015.
[22] B. Soykan and G. Rabadi, "A Tabu search algorithm for the multiple runway aircraft scheduling problem," in *Heuristics, Metaheuristics and Approximate Methods in Planning and Scheduling*. Cham, Switzerland: Springer, 2016, pp. 165–186.
[23] Z.-H. Zhan, J. Zhang, Y. Li, O. Liu, S. K. Kwok, W. H. Ip, and O. Kaynak, "An efficient ant colony system based on receding horizon control for the aircraft arrival sequencing and scheduling problem," *IEEE Trans. Intell. Transp. Syst.*, vol. 11, no. 2, pp. 399–412, Jun. 2010.
[24] G. Bencheikh, J. Boukachour, and A. E. H. Alaoui, "Improved ant colony algorithm to solve the aircraft landing problem," *Int. J. Comput. Theory Eng.*, vol. 3, no. 2, pp. 224–233, 2011.
[25] M. Brittain and P. Wei, "Autonomous aircraft sequencing and separation with hierarchical deep reinforcement learning," in *Proc. Int. Conf. Res. Air Transp.*, Barcelona, Spain, 2018, pp. 1–10.
[26] P. Zhao and Y. Liu, "Physics informed deep reinforcement learning for aircraft conflict resolution," *IEEE Trans. Intell. Transp. Syst.*, vol. 23, no. 7, pp. 8288–8301, Jul. 2021.
[27] J. C. Jones, D. J. Lovell, and M. O. Ball, "Stochastic optimization models for transferring delay along flight trajectories to reduce fuel usage," *Transp. Sci.*, vol. 52, no. 1, pp. 134–149, Jan. 2018.
[28] A. Khassiba, F. Bastin, B. Gendron, S. Cafieri, and M. Mongeau, "Extended aircraft arrival management under uncertainty: A computational study," *J. Air Transp.*, vol. 27, no. 3, pp. 131–143, Jul. 2019.
[29] A. Khassiba, F. Bastin, S. Cafieri, B. Gendron, and M. Mongeau, "Two-stage stochastic mixed-integer programming with chance constraints for extended aircraft arrival management," *Transp. Sci.*, vol. 54, no. 4, pp. 897–919, Jul. 2020.
[30] A. Khassiba, S. Cafieri, F. Bastin, M. Mongeau, and B. Gendron, "Two-stage stochastic programming models for the extended aircraft arrival management problem with multiple pre-scheduling points," *Transp. Res. C, Emerg. Technol.*, vol. 142, Sep. 2022, Art. no. 103769.
[31] M. Schultz, D. Lubig, E. Asadi, J. Rosenow, E. Itoh, S. Athota, and V. N. Duong, "Implementation of a long-range air traffic flow management for the Asia–Pacific region," *IEEE Access*, vol. 9, pp. 124640–124659, 2021.
[32] L. Zhi Jun, S. Alam, I. Dhief, and M. Schultz, "Towards a greener extended-arrival manager in air traffic control: A heuristic approach for dynamic speed control using machine-learned delay prediction model," *J. Air Transp. Manage.*, vol. 103, Aug. 2022, Art. no. 102250.
[33] E. Itoh and M. Mitici, "Queue-based modeling of the aircraft arrival process at a single airport," *Aerospace*, vol. 6, no. 10, p. 103, Sep. 2019.
[34] E. Itoh and M. Mitici, "Analyzing tactical control strategies for aircraft arrivals at an airport using a queuing model," *J. Air Transp. Manage.*, vol. 89, Oct. 2020, Art. no. 101938.

[35] E. Itoh and M. Mitici, "Evaluating the impact of new aircraft separation minima on available airspace capacity and arrival time delay," *Aeronaut. J.*, vol. 124, no. 1274, pp. 447–471, Apr. 2020.
[36] K. Higasa, K. Sekine, and E. Itoh, "Effectiveness of aircraft inter-arrival control in upstream traffic flow via a combined tandem fluid queue model and integer programming approach," *IEEE Access*, vol. 11, pp. 15252–15270, 2023.
[37] *Passenger Traffic 2017 Final (Annual)*, Airports Council International (ACI), Montreal, QC, Canada, 2019.
[38] The International Air Transport Association (IATA). (2022). *Worldwide Airport Slot Guidelines (WASG)*. [Online]. Available: https://www.iata.org/en/programs/ops-infra/slots/slot-guidelines/
[39] *Point Merge in Extended Terminal Area*, Eurocontrol, Brussels, Belgium, 2010.
[40] K. Sekine, F. Kato, K. Kageyama, and E. Itoh, "Data-driven simulation for evaluating the impact of lower arrival aircraft separation on available airspace and runway capacity at Tokyo international airport," *Aerospace*, vol. 8, no. 6, p. 165, Jun. 2021.
[41] *The Procedures for Air Navigation Services—Air Traffic Management*, International Civil Aviation Organization (ICAO), Montreal, QC, Canada, 2016.
[42] *The Procedures for Air Navigation Services—Air Traffic Management*, International Civil Aviation Organization (ICAO), Montreal, QC, Canada, Nov. 2020.
[43] K. Sekine, T. Tatsukawa, E. Itoh, and K. Fujii, "Multi-objective take-off time optimization using cellular automaton-based simulator," *IEEE Access*, vol. 9, pp. 79461–79476, 2021.
[44] L. Breiman, J. Friedman, R. Olshen, and C. Stone, "Cart," in *Classification and Regression Trees* . Monterey, CA, USA: Wadsworth and Brooks/Cole, 1984.
[45] K. Deb, A. Pratap, S. Agarwal, and T. Meyarivan, "A fast and elitist multiobjective genetic algorithm: NSGA-II," *IEEE Trans. Evol. Comput.*, vol. 6, no. 2, pp. 182–197, Apr. 2002.
[46] A. Vanwelsenaere, J. Ellerbroek, J. Hoekstra, and E. Westerveld, "Effect of popup flights on the extended arrival manager," *J. Air Transp.*, vol. 26, pp. 1–10, Jun. 2018.
[47] T. S. Abbott, "An overview of a trajectory-based solution for en route and terminal area self-spacing: Seventh revision," NASA, Washington, DC, USA, Tech. Rep., CR-2015-218794, 2015.
[48] B. T. Baxley, K. A. Swieringa, S. R. Wilson, R. D. Roper, T. S. Abbott, C. E. Hubbs, P. Goess, and R. F. Shay, "Air traffic management technology demostration-1 (ATD-1) avionics phase 2 flight test and results," NASA, Washington, DC, USA, Tech. Rep., TP-2018-219814, 2018.
[49] EUROCONTROL. (2015). *Base of Aircraft Data (BADA)*. [Online]. Available: https://www.eurocontrol.int/sites/default/files/publication/files/bada-factsheet.pdf
[50] K. Pearson, "Mathematical contributions to the theory of evolution.-III. Regression, heredity, and panmixia," *Phil. Trans. Roy. Soc. London, A*, vol. 187, pp. 253–318, Jan. 1896.
[51] AirtopSoft. *Airtop Software*. Accessed: Feb. 22, 2020. [Online]. Available: https://airtopsoft.com/

KATSUHIRO SEKINE received the B.E. and M.E. degrees from the Industrial Management and Engineering, Tokyo University of Science, Japan, in 2019 and 2022, respectively, where he is currently pursuing the Ph.D. degree with the Department of Information and Computer Technology. During his undergraduate career, he visited the German Aerospace Center (DLR), as a Research Trainee and carried out research on extended arrival management. He is also a Research Trainee with the Air Traffic Management Department, Electronic Navigation Research Institute, National Institute of Maritime, Port and Aviation Technology. His research interests include multi-objective optimization, statistical and machine learning methods, modeling and simulation, and their applications to air traffic management.

FURUTO KATO received the B.S. degree in aeronautics and astronautics from The University of Tokyo, Japan, in 2021, where he is currently pursuing the master's degree. He has recently completed a graduation thesis about estimating the maximum runway capacity and arrival delays at Tokyo International Airport using stochastic data analysis and queuing models. His research interests include ATC and automation of air traffic management and their impact on airport operations and controller workload.

TOMOAKI TATSUKAWA (Member, IEEE) received the B.S. degree and the M.S. degree in engineering from the Tokyo Institute of Technology, Tokyo, Japan, in 2002 and 2004, respectively, and the Ph.D. degree in engineering from The University of Tokyo, Tokyo, in 2012. He was a Software Engineer with SGI Japan Ltd., from 2004 to 2010. From 2012 to 2015, he was a Postdoctoral Research Fellow with the Institute of Space and Astronautical Science, Japan Aerospace Exploration Agency (ISAS/JAXA), Sagamihara, Japan. From 2015 to 2019, he was a Junior Associate Professor with the Tokyo University of Science, Tokyo, where he has been an Associate Professor with the Department of Information and Computer Technology, since April 2020. His research interests include multi-objective evolutionary computation, aerodynamic design optimization, and multi-objective design exploration. He is a member of JSME. He received the Young Researcher Award from the IEEE Computational Intelligence Society Japan Chapter, in 2011.

KOZO FUJII (Member, IEEE) received the Ph.D. degree in engineering from The University of Tokyo, Tokyo, Japan, in 1980. He was a NRC Research Associate with the NASA Ames Research Center, USA, from 1981 to 1983. He was a Senior Research Scientist with the National Aerospace Laboratory, Chofu, Japan, from 1984 to 1988. He was an Associate Professor with the Institute of Space and Astronautical Science, Japan Aerospace Exploration Agency (ISAS/JAXA), Sagamihara, Japan, from 1988 to 1997. He was a Professor with ISAS/JAXA, from 1997 to 2015. Since April 2015, he has been a Professor with the Tokyo University of Science, Tokyo. His research interests include aero-acoustics and flow control. He has been a fellow of AIAA, since 2004. He is one of the 210 members of "Science Council of Japan." He received many awards, such as the Daniel and Florence Guggenheim Award from the International Council of the Aeronautical Sciences, in 2004. He served on the editorial board of many journals.

ERI ITOH received the Ph.D. degree in aeronautics and astronautics from The University of Tokyo, Japan, in 2007. After gaining experience in international research organizations, she currently holds the positions of a Professor with the Research Center for Advanced Science and Technology and the Aeronautics and Astronautics Department, The University of Tokyo, and a Chief Researcher with the Air Traffic Management Department, Electronic Navigation Research Institute, National Institute of Maritime, Port and Aviation Technology. Combining data-driven analysis, mathematical models and simulation studies, she works toward realizing even more efficient and resilient air traffic operations. Her research interests include the design of automation systems that work with human operators in air traffic management, including airspace and airport operation.